Methacrylated cellulose nanocrystals as fillers for the development of photo-crosslinkable cytocompatible biosourced formulations targeting 3D printing

Lénaïc Soullard, Flavie Pradalié, Béatrice Labat, Christine Lancelon-Pin, Guillaume Nonglaton, Sébastien Rolere, Isabelle Texier, Bruno Jean

Methacrylated cellulose nanocrystals as fillers for the development of photo-crosslinkable cytocompatible biosourced formulations targeting 3D printing

Lénaïc Soullard,[a,b,c] Flavie Pradalié,[c] Béatrice Labat,[d] Christine Lancelon-Pin,[c] Guillaume Nonglaton,[b] Sébastien Rolere,[a] Isabelle Texier[b] and Bruno Jean[c]*

[a] *Univ. Grenoble Alpes, CEA, LITEN, DTNM, Grenoble, France*

[b] *Univ. Grenoble Alpes, CEA, LETI, DTBS, Grenoble, France*

[c] *Univ. Grenoble Alpes, CNRS, CERMAV, Saint-Martin-d'Hères, France*

[d] *Univ. Rouen Normandie, INSA Rouen Normandie, CNRS, PBS, Evreux, France*

KEYWORDS: Carboxymethylcellulose, cellulose nanocrystals, methacrylation, photo-crosslinking, hydrogel, cytotoxicity

ABSTRACT

Cellulose nanocrystals (CNCs) from cotton were functionalized in aqueous medium using methacrylic anhydride (MA) to produce methacrylated cellulose nanocrystals (mCNCs) with a degree of methacrylation (DM) up to 12.6 ± 0.50 %. Dispersible as-prepared CNCs and mCNCs were then considered as reinforcing fillers for aqueous 3D-printable formulations based on

methacrylated carboxymethylcellulose (mCMC). The rheological properties of such photo-crosslinkable aqueous formulations containing non-modified CNCs or mCNCs at 0.2 or 0.5 wt% in 2 wt% mCMC were fully investigated. The influence of the presence of nanoparticles on the UV-curing kinetics and dimensions of the photo-crosslinked hydrogels was probed and ^{13}C CP-MAS NMR spectroscopy was used to determine the maximum conversion ratio of methacrylates as well as the optimized time required for UV post-curing. The viscoelasticity of crosslinked hydrogels and swollen hydrogels was also studied. The addition of 0.5 wt% mCNC with a DM of 0.83 ± 0.040 % to the formulation yielded faster crosslinking kinetics, better resolution, more robust crosslinked hydrogels and more stable swollen hydrogels than pure mCMC materials. Additionally, the produced cryogels showed no cytotoxicity toward L929 fibroblasts. This biobased formulation could thus be considered for the 3D printing of hydrogels dedicated to biomedical purposes using vat polymerization techniques such as stereolithography or digital light processing.

1. INTRODUCTION

Three-dimensional printing technologies based on vat polymerization of liquid resins, such as stereolithography (SLA) or digital light processing (DLP), have very interesting resolutions of around 30-50 µm.[1] In recent years, thanks to these characteristics, these methods were increasingly used to print innovative medical devices, such as implantable scaffolds for tissue engineering and drug delivery systems.[2–4] Indeed, medical applications require very precise manufacturing processes to adapt the devices' dimensions to those of human tissues, for example.[4] Nevertheless, the 3D printing of medical devices with vat technologies requires the availability of biocompatible and photo-crosslinkable liquid resins. Moreover, the 3D-printed objects should advantageously be bioresorbable to enable targeting implantable applications,

such as bone repair.[5] Natural polymers that benefit from inherent biocompatibility and bioresorbability thus meet the criteria for developing such liquid formulations, provided they can be photo-crosslinked.[6,7]

In this context, many cellulose derivatives with various characteristics have already been investigated for 3D printing applications.[8–10] Among these, carboxymethylcellulose (CMC) is probably one of the most studied biosourced polymers for biomedical applications thanks to its water solubility[11,12] and ability to be chemically modified with (meth)acrylate groups by reaction with methacrylic anhydride to make it photo-crosslinkable.[13–16]

When solubilized in water in the presence of a biocompatible photoinitiator,[17] methacrylated carboxymethylcellulose (mCMC) can be shaped into a crosslinked hydrogel by UV-curing.[16,18,19] The resulting materials are three-dimensional mCMC networks with entrapped water that are currently considered for biomedical applications such as cell encapsulation,[19] tissue engineering[20] or drug delivery.[15] Unfortunately, the UV-curing of molded mCMC resins usually does not allow manufacturing hydrogels with complex shapes. Vat polymerization 3D printing techniques have therefore recently been proposed to enhance the shape complexity of mCMC hydrogels.[18] However, the resolution of the objects prepared in this work using DLP is still limited (around 500 µm). A usual strategy to improve the resolution of printed objects is the addition of a photo-absorber to limit the transmission of the UV-light throughout the formulation during insolation.[21–23] In the case of aqueous mCMC formulations for biomedicine, the ideal photo-absorber must be biocompatible, soluble or dispersible in water, and should absorb at a specific wavelength (typically 365, 385 or 405 nm). However, the known photo-absorbers meeting these last two criteria fail to exhibit biocompatibility,[21] some of them being even suspected to be toxic, such as tartrazine used for yellow food coloring.[24]

Additionally, when the concentration of photosensitive groups in the initial formulation is low, crosslinked hydrogels often display poor mechanical properties, that are insufficient for use as

biological tissue scaffolds.[25,26] In order to address this problem, the integration in the formulation of cellulose nanocrystals (CNCs) as reinforcing fillers can be considered. CNCs are biocompatible cellulose nanorods most commonly obtained by sulfuric acid hydrolysis of a wide variety of cellulose sources that display exceptional mechanical properties, such as a tensile strength of about 10 GPa.[27–29] Since the pioneering work of Favier and coworkers[30], CNCs have widely been considered as reinforcing fillers in nanocomposites, including biocomposites.[31,32] In the case of photo-crosslinked CMC hydrogels, strong interactions between the hydrophilic parts of mCMC and the surface of cellulose nanocrystals can be expected, both materials comprising a cellulose backbone enabling hydrogen bonds to form.[33,34] Moreover, the dispersion in water of the crystalline cellulose nanorods should allow limiting the transmission of the light beam, especially for wavelengths comparable to their size.[35]

In the present paper, the introduction of CNCs into photo-crosslinkable and printable mCMC formulations has been studied to limit the UV-light transmission in the formulations during insolation, but also to improve the mechanical properties of the final hydrogels. Cellulose nanorods were either used as-prepared after acid hydrolysis, or in the form of methacrylated nanocrystals (mCNC) as previously described by Cafiso et al.[36] Several methods of methacrylation of CNCs have been reported in the last past years,[37–39] in particular through the reaction with methacrylic anhydride (MA) in organic solvents.[40–43] In the present work, to avoid the use of such solvents, CNCs were methacrylated with MA in aqueous medium using the same conditions as we recently reported for the methacrylation of CMC.[16] This particular reaction was already applied to cellulose nanofibrils (CNFs),[44] and once to CNCs,[45] but in the latter case only a few details were reported about the characterization of the resulting functionalized materials. Here, after quantifying and optimizing the methacrylation of the CNCs, the influence of mCNCs on the formulations and prepared hydrogels was investigated

in terms of visco-elastic properties and crosslinking density. Finally, a cytotoxicity evaluation was performed on cryogels obtained upon hydrogel freeze-drying.

2. EXPERIMENTAL SECTION

2.1. Materials. Sulfuric acid 98%, Ethanol 96%, methacrylic anhydride (MA) containing 2,000 ppm topanol A as inhibitor, 2-hydroxy-4′-(2-hydroxyethoxy)-2-methylpropiophenone (Irgacure 2959) and anhydrous sodium hydroxide pellets were purchased from Sigma Aldrich (France) and used as received. Sodium salt of CMC (NaCMC, reference BLANOSE 7LP EP, a king gift from Ashland, France) with a weight-average molar mass of 90.5 kg.mol^{-1} and a degree of substitution of 0.7 was used as received. Cotton linters were purchased from Buckeye Cellulose Corporation (US). L929 fibroblasts (CCL-1^{TM}) were obtained from ATCC® (LGC Standards, UK), α-Minimum Essential Medium (α -MEM), streptomycin/penicillin and L-glutamine were purchased from Sigma Aldrich (France) and fetal bovine serum (FBS) from Gibco (Gibco-BRL, USA). Live/Dead kit was purchased from Molecular Probes (Invitrogen, USA).

2.2. Preparation of cellulose nanocrystals from cotton. The protocol of CNC production was based on the work of Revol et al.[46] Cotton linters (60 g) were cut in small pieces and mixed with a blender. The acid hydrolysis was carried out in 64 wt% sulfuric acid in water (840 ml) at 60 °C during 30 min under mechanical stirring. The hydrolysis was stopped by adding a volume of ice representing 50 wt% of the volume of the acid solution. Sulfuric acid was removed by centrifugation at 20,300 g and 4 °C during 30 min using a Sigma 6-16KS centrifuge (SIGMA, Germany). After redispersion of the sediment containing CNCs in deionized water during 30 min, a centrifugation was performed during 15 min at 20,300 g and 20 °C and the supernatant was discarded. This sequence was repeated three times. The resulting mixture was dispersed in 2 L of water and purified for 10 days by dialysis against deionized water using a

cellulose-mixed ester membrane (MWCO = 12-14 kg/mol; Roth, Germany) until the conductivity of the water bath was equal to that of deionized water. The suspension was then ultra-sonicated using a Branson 450 Digital Sonifier (Emerson, France) during 5 min using a pulse mode to limit heating. During sonication, the beaker containing the dispersion was also placed in an ice bath to prevent any temperature increase. The suspension was then filtered through a 5 µm then a 1 µm Whatman cellulose nitrate membrane with a Sartorius filtration equipment to remove large aggregates. The concentration of CNCs in the final aqueous suspension (2.3 wt%) was measured from the dry extract.

2.3. Methacrylation of cellulose nanocrystals. Methacrylic anhydride (MA) was added dropwise to 100 g of a 2 wt% dispersion of CNCs in deionized water. Molar ratios of 3.0, 6.0, 12 or 24 between MA and CNC surface hydroxyl groups ($N_{MA}/N_{OH(surf)}$) were used. The number of hydroxyl groups on the surface of CNCs, $N_{OH(surf)}$, was calculated using equation 1 proposed by Eyley et Thielemans.[46]

$$N_{OH(surf)} = \frac{n_1+n_2}{\rho N_A L_1 L_2 c}\left(\frac{L_1+L_2}{d_{(110)}}+\frac{L_1+L_2}{d_{(1\bar{1}0)}}\right)+2(\rho N_A L_3 d_{(110)} d_{(1\bar{1}0)})^{-1} \quad (1)$$

where n_1 (=2) and n_2 (=4) are the number of primary and secondary hydroxyl groups in two consecutive anhydroglucose units, respectively, ρ is the crystalline cellulose density (1.605 g/cm^3), N_A is Avogadro's number (6.022x10^{23} mol^{-1}), c is the unit cell dimension (1.038 nm), and L_1, L_2 and L_3 are respectively the width (22 nm), the height (6 nm) and the length (150 nm) of cotton nanocrystals extracted from small-angle neutron scattering experiments.[48] The interplane distances d(110) and d(1$\bar{1}$0) are 0.53 and 0.59 nm, respectively. [49] This calculation gave an $N_{OH(surf)}$ value of 4.59x10^{-3} mol/g.

During the 24h reaction at room temperature, the pH was constantly adjusted to 8 with a 10 N NaOH solution and magnetic stirring was used. After the reaction, the methacrylated

nanocrystals (mCNCs) were precipitated in 200 mL ethanol and centrifuged at 16,200 g and 20 °C during 15 min with a Sigma 6-16KS centrifuge (SIGMA, Germany). mCNC were then redispersed in 100 mL of water and centrifuged at 16,200 g and 20 °C for 30 min. The resulting mixture was dispersed in 100 mL of water and purified for 7 days by dialysis against deionized water using a cellulose-mixed ester membrane (MWCO = 12-14 kg/mol; Roth, Germany). Then, the mCNC product was freeze-dried for 3 days with a CHRIST Beta 2-8 LS plus lyophilizer (Martin Christ Gefriertrocknungsanlagen, Germany). Part of the recovered mCNC solid was dispersed at 1 wt% in deionized water by ultra-sonication using a Branson sonifier during 7 min by alternating 50 s of sonication and 50 s of break. The beaker containing dispersion was placed in an ice-bath during sonication to prevent any temperature increase.

2.4. Methacrylation of carboxymethylcellulose. Methacrylated carboxymethylcellulose (mCMC) was synthesized as previously reported.[16] NaCMC was solubilized at 2 wt% in deionized water at room temperature under mechanical stirring at 2,000 rpm, with an anchor-shaped glass pall. MA was then added dropwise to the CMC solution with a molar ratio of 1.2 between MA and CMC hydroxyl groups. The reaction was continued for 24 h at room temperature. The pH was constantly adjusted to 8 with a 10 M NaOH solution during the reaction. The resulting mixture was purified during 7 days by dialysis against deionized water using a cellulose mixed-ester membrane (MWCO = 12-14 kg/mol; Roth, Germany). Then, the mCMC product was freeze-dried for 5 days with a CHRIST Beta 2-8 LS plus lyophilizer (Martin Christ Gefriertrocknungsanlagen, Germany).

2.5. Preparation and photo-crosslinking of aqueous mCMC formulations. Aqueous formulations containing 2 wt% of mCMC, and 0.2 or 0.5 wt% CNCs or mCNCs were prepared. The mixture was magnetically stirred for 12 h at 50 °C. The photoinitiator Irgacure 2959 was then added at room temperature, with a constant molar ratio of 0.55, compared to the total number of moles of methacrylates in the formulations. This photoinitiator was selected because

it is water-soluble (0.5 wt% maximum), non-toxic and absorbs at 365 nm.[17] The formulations were then stirred using a multi-rotator PTR-35 (Grant, UK) at 6 rpm for 12 h at room temperature. 650 µL of each formulation were placed in a PTFE circular mold of 15 mm in diameter and 1 cm in height and then insolated for 5 min under a UV-light source at a wavelength of 365 nm and an irradiance of 82 mW/cm². All resulting hydrogels had a thickness of 3.6 mm and a diameter of 15 mm. To yield cryogels, the hydrogel samples were set in an aluminum basket, filled with liquid nitrogen and freeze-dried overnight with a CHRIST Beta 2-8 LS plus lyophilizer (Martin Christ Gefriertrocknungsanlagen, Germany).

In another experiment aiming at evaluating the resolution of the hydrogels in all three directions (x, y and z), a volume corresponding to 1 cm in height of formulation was set in an aluminum cup. Then, a black template with a 12 mm diameter hole was placed on the surface (Supporting Information Figure S1). Insolation at different times was controlled by the lamp module. The obtained crosslinked hydrogel piece was taken off from the formulation, and its width and thickness were measured with a caliper at different positions. The same procedure was done with a star-shaped template to measure the hydrogel resolution.

2.6. NMR spectroscopy.

2.6.1. ^{1}H NMR spectroscopy. ^{1}H NMR spectroscopy was used to quantify the degree of methacrylation (DM) of the mCMC samples. The DM corresponds to the number of methacrylate groups per 100 anhydroglucose units of mCNC. 4.5 mg of mCMC were dissolved in 650 µL of D_2O at 50 °C for 12 h using a ThermoMixer C (Eppendorf, Germany). All ^{1}H NMR spectra were recorded on a Spectrospin 300 MHz spectrometer (Bruker, Germany) at 25 °C from 64 successive scans with a relaxation time D1 of 3 s.

2.6.2. ^{13}C cross-polarization magic-angle spinning (CP-MAS) solid-state nuclear magnetic resonance (NMR) spectroscopy. ^{13}C CP-MAS solid-state NMR was used to quantify the degree

of methacrylation of the mCNC and mCMC samples. The same technique was used to determine the conversion rate of methacrylates upon photo-crosslinking and calculate the cross-linked methacrylate and the free methacrylate densities in the pure mCMC or composite cryogels. 80 mg of CNC, mCNC or cross-linked cryogel were crushed and set in a 3 mm diameter rotor. All CP-MAS solid-state NMR spectra were recorded on a Neo 500 MHz spectrometer (Bruker, Germany) operating at 125.8 MHz. The acquisition time was 28 ms, the sweep width was 37 kHz, the contact time was 2 ms and at least 4,096 successive scans were recorded at 25 °C.

2.7. Conductometric titration. Conductometric titration was used to determine the amount of sulfate half esters (DS) at the surface of the CNCs just after their preparation by sulfuric acid hydrolysis and that of mCNC after methacrylation, as described by Darpentigny et al.[50] A suspension of 2.3 wt% of CNC or mCNC in water was titrated with 0.01 M NaOH and the sulfate content was extracted using equation 2:

$$DS = \frac{V_{eq} \times C_{NaOH} \times M_{mean}}{m_{cellulose}} \quad (2)$$

Where V_{eq} is the volume (in L) of NaOH necessary for the titration of the CNC or mCNC suspension, C_{NaOH} the concentration of NaOH (0.01 M), $m_{cellulose}$ the mass of titrated CNC or mCNC (in g), and M_{mean} the mean molar mass of one repetitive unit considering sulfates (in g/mol), calculated by equation 3:

$$M_{mean} = \frac{M_{glu}}{1-(M_{glu+sulf}-M_{glu}) \times \left(V_{eq} \times \frac{C_{NaOH}}{m_{cellulose}}\right)} \quad (3)$$

Where M_{glu} is the molar mass of the repetitive unit of cellulose (162 g/mol) or the molar mass of the repetitive unit of methacrylated cellulose, $M_{glu+meth}$, that takes into account the DM value of the considered mCNC sample and is given by equation 4

$$M_{glu+meth} = (1 - DM) \times 162 + DM \times 231 \quad (4)$$

In equation 3, $M_{glu+sulf}$ is the molar mass of the repetitive unit of cellulose with a sulfate half ester group at C6 position (242 g/mol). For mCNCs, the average molar mass of a glucose unit with a methacrylate is 231 g/mol.

2.8. Dynamic Light Scattering (DLS). Dynamic light scattering experiments were carried out with a Zetasizer Nano ZS (Malvern, UK) at 25 °C to determine the intensity size distribution of the nanorods. The instrument operated with a 2 mW HeNe laser at a wavelength of 632.8 nm and with a detection angle of 173°. The CNC and mCNC nanorods were characterized at a concentration of 0.1 wt% in water. The medium viscosity was fixed to that of water at 25 °C (0.8872 mPa.s), the medium refractive index to 1.33, and material refractive index to 1.50 corresponding to that of CNC at 632.8 nm.[51] The sample was loaded into a quartz microcuvette (3.5 mL, l = 1 cm), and three measurements of 13 runs each were averaged.

2.9. UV-vis spectroscopy. UV-vis spectra of aqueous formulations containing mCMC and CNC or mCNC, without photoinitiator, were recorded from 350 to 800 nm with a Cary 300 UV-visible spectrophotometer (Varian, US). The formulations were placed in a polystyrene cuvette (1 mL, light path = 1 cm). The baseline was previously recorded with deionized water in the same cuvette.

2.10. Scanning electron microscopy (SEM). SEM was used to investigate the cryogel morphology and measure the pore size distribution. Samples were fractured horizontally and pasted on metallic stubs with carbon cement, fractured and sputter-coated with Au/Pd. Secondary electron images were recorded with a FEI Quanta 250 (Thermo Fisher Scientific, US) scanning electron microscope equipped with a field emission gun operating at 2.5 kV. All pores were observed on the fractured surface. The pore size was determined by image treatment

using the ImageJ software. Horizontal or vertical lines were drawn on each pore, giving the average pore size. This procedure was performed on 25 pores per image and 4 images per sample. Pores whose walls were broken by the cutting method were not measured.

2.11. Transmission electron microscopy (TEM). Droplets of dilute CNC and mCNC aqueous suspensions were deposited onto glow-discharged carbon-coated copper grids and negatively stained with 2 wt% uranyl acetate. The specimens were observed with a JEOL JEM-2100-Plus microscope operating at an accelerating voltage of 200 kV. Images were recorded with a Gatan Rio 16 camera.

2.12. Rheology measurement.

2.12.1. Rheometer instrument. The viscosity measurements, gelation time of formulations under UV-light, and rheological properties of hydrogels were measured using a Kinexus Pro+ parallel plate rheometer (Netzsch, Germany).

2.12.2. Viscosity measurements. Shear rate measurements were performed from 0.1 to 100 s^{-1} at 25 °C. Steel parallel plates with 0.2 mm gap and 50 mm diameter were used. All the experiments were carried out at least on two different samples.

2.12.3. Real-time (RT-) rheology. Rheology measurements were performed in real-time during UV insolation that was manually controlled using a UFIBER-COL UV fiber lamp 365 nm (UWAVE, France). The formulations were deposited on a UV-transparent quartz plate. The mobile plane had a diameter of 20 mm and the gap between this plane and the quartz plate was 0.2 mm. The UV lamp was adjusted and placed underneath the quartz plate at a distance yielding an exposure of 2 cm in diameter with an average power density of 82 mW/cm². The elastic (G') and viscous (G'') shear moduli were measured over time with a 5 % strain, at 0.1 Hz and at room temperature. After 1 minute of stabilization without UV irradiation, the radiation

was turned on during 10 minutes. All the experiments were carried out on three different samples.

2.12.4. Rheological properties of photo-crosslinked hydrogels. Frequency sweep measurements were performed at a constant temperature (25 °C) from 0.1 to 10 Hz. According to preliminary amplitude sweep measurements, all tests were carried out in the linear viscoelastic region at 1 % strain. The gap between the plate and the mobile plane (20 mm diameter) was set to 0.4 mm. All the experiments were carried out on three different samples.

2.13. Swelling ratio. Swelling tests were performed on three different hydrogels per condition. The samples were immersed in deionized water at room temperature. The swollen hydrogels were regularly weighed at increasing times, t, until mass equilibrium was reached, in order to determine the swelling ratio (SR) according to equation 5:

$$SR = w_t / w_0 \quad (5)$$

where w_0 is the initial hydrogel weight and w_t is the weight of the swollen hydrogel at measurement time t. The swollen hydrogels were freeze-dried and transformed into cryogels. Cryogel masses were measured and compared with the ones obtained from the initial hydrogels after photo-crosslinking.

2.14. Cytotoxicity assay. *2.14.1. Samples sterilization.* Prior to cytotoxicity evaluation, all cryogels were sterilized in an ethanol/water (70/30 wt%) bath for 24h under gentle rotary shaking. Then, they were moved into sterile Ultrapure water (Milli-Q – 18.2 MΩ.cm) for an additional 24h to eliminate ethanol and finally transferred into a complete cell culture medium composed of α-MEM supplemented with 10% FBS, streptomycin/penicillin (100 $mg.mL^{-1}$/100 mM respectively) and 2 mM L-glutamine, for at least 48h and kept as such in sterile conditions until used.

2.14.2. Cell culture conditions. L929 mouse fibroblast cells were routinely grown into 75 cm^2 plastic tissue culture flasks, with the same complete culture medium as described above and incubated in a controlled humidified atmosphere with 5% CO_2 at 37°C. When subconfluent, cells were enzymatically detached using 0.25% trypsin–1 mM EDTA (Sigma).

2.14.3. Cytotoxicity evaluation. The cytotoxicity of the different formulations was assessed according to ISO 10993-5 2009 with some adaptations.[52] Briefly, two tests were performed: *in situ* elution and direct contact. Samples were carefully distributed into 12-well plates with the help of sterile tweezers. Then, L929 cells were seeded on the bottom of the wells (*in situ* elution test) and on top of the samples (direct contact test), at a density of $50x10^3$ cells per cm^2, and let grown for 48h. DMSO (10%) and complete cell culture medium were used as positive (Ctrl +) and negative (Ctrl -) controls of toxicity, respectively.

For the *in situ* elution test, a morphological inspection of cells that adhered all around the samples on the bottom of the wells was carried out by using a phase contrast inverted microscope (Motic, China).

For the direct contact test, we first checked cell viability by using the Live/Dead® kit composed of two fluorogenic products. Calcein AM, an esterase substrate, gives a green-fluorescence when hydrolyzed, indicating that cell membranes are not damaged and that cells are viable. Ethidium homodimer-1, a red-fluorescent nucleic acid fluorophore, reveals damaged cell membranes since this compound should normally not penetrate into cells. Subsequently, viable cells are stained green while damaged/dead cells appear red. Cells were imaged by using a Zeiss Axio Scope A1 epifluorescence microscope (Carl Zeiss, Germany) equipped with a CCD camera (Motic, China). In parallel, we investigated the cell metabolic activity by using Alamar Blue® assay (AB – Bio-Rad, UK) over a 7-days culture period. This common quantitative indicator of cell viability assay is based on the oxidation-reduction reactions that occur in cell mitochondria. At D2, D5 and D7 days, the complete culture medium was replaced by 10% (v/v)

AB-containing culture medium for 3h. Then, absorbance measurements were carried out at 570 and 600 nm with a microplate reader (BioTeck – Synergy 2, USA).

3. RESULTS AND DISCUSSION

3.1. Methacrylation of cellulose nanocrystals (CNC). Photo-crosslinkable methacrylate groups were grafted onto CNCs using the reaction between methacrylic anhydride and surface hydroxyl groups (Figure 1a) following the procedure we developed previously for carboxymethylcellulose methacrylation.[16] The reaction was conducted at room temperature, instead of 50 °C as proposed by Ma et al., as the temperature was not influencing the methacrylation in our previous work.[16] The influence of the molar ratio between MA and CNC surface hydroxyl groups, $N_{MA}/N_{OH(surf)}$, on the degree of methacrylation (DM) and the methacrylation kinetics were studied.

All mCNC samples were characterized by ^{13}C CP-MAS solid-state NMR spectroscopy and compared to as-prepared CNCs (Figure 1b). According to the literature, CNC carbons (C1-C6) are located from 56 ppm to 110 ppm.[53] Carbon C1 presents the higher chemical shift at 104 ppm, and the peak splitting corresponds to cotton's Iβ cellulose crystallographic structure. [54] The signal at 89 ppm was attributed to C4 carbons inside the CNC crystalline structure, while the signal at 84 ppm corresponds to C4 carbons at the surface of the crystals.[55] C2, C3 and C5 signals are located between 68 and 80 ppm, and C6 signal at 65 ppm. As with C4, the latter featured amorphous and crystalline CNC domains that would require peak deconvolution. For mCNC samples, four additional peaks corresponding to the carbonyl (C7: 167 ppm), vinyl (C8: 136 ppm and C9: 127 ppm) and methyl (C10: 18 ppm) carbons of the methacrylate groups were observed after purification, indicating that surface methacrylation occurred under our experimental conditions, as observed by Wang et al.[39] for CNC methacrylation using methacrylic acid (Figure 1b). Interestingly, the comparison of the C4 signals of the CNC and

mCNC spectra evidenced no significant variation in the CNC amorphous and crystalline ratios, indicating that the crystal structure was not altered during the methacrylation. The crystallinity index was calculated as the ratio between the integral of the crystalline $C4_{cr}$ peak (82 – 94 ppm) and the total integral of the C4 domain (76 – 94 ppm) using deconvolution (Figure 1c).[56,57] The crystallinity index of 68 % calculated for both CNC and mCNC, was in good agreement with the values reported for cellulose nanocrystals from cotton obtained by sulfuric acid hydrolysis.[56,58] This result demonstrates that the surface-to-volume ratio of the particles was preserved during the reaction. In other words, the methacrylation reaction only occurred on the surface of the CNCs. Finally, integrating carbon C1 as a reference with a value of 1, the integration of carbon C4 gave an area of 1 and the integration of carbons C2, C3, C5 and C6 between 50 and 94 ppm gave an area of 4, indicating that the polarization of these carbons was optimized using the acquisition parameters of these ^{13}C CP-MAS NMR spectra (Supporting Information Figure S2). The degree of methacrylation (DM) of mCNC samples was then calculated from the C10 signal. Carbon C10 corresponding to the CH_3 of the methacrylate groups is indeed more mobile and consequently more suitable for DM quantification than unsaturated carbons C7-9.[59] In addition, the polarization of C10 carbons reaches a maximum value for the contact time used (2 ms) (Supporting Information Figure S2).

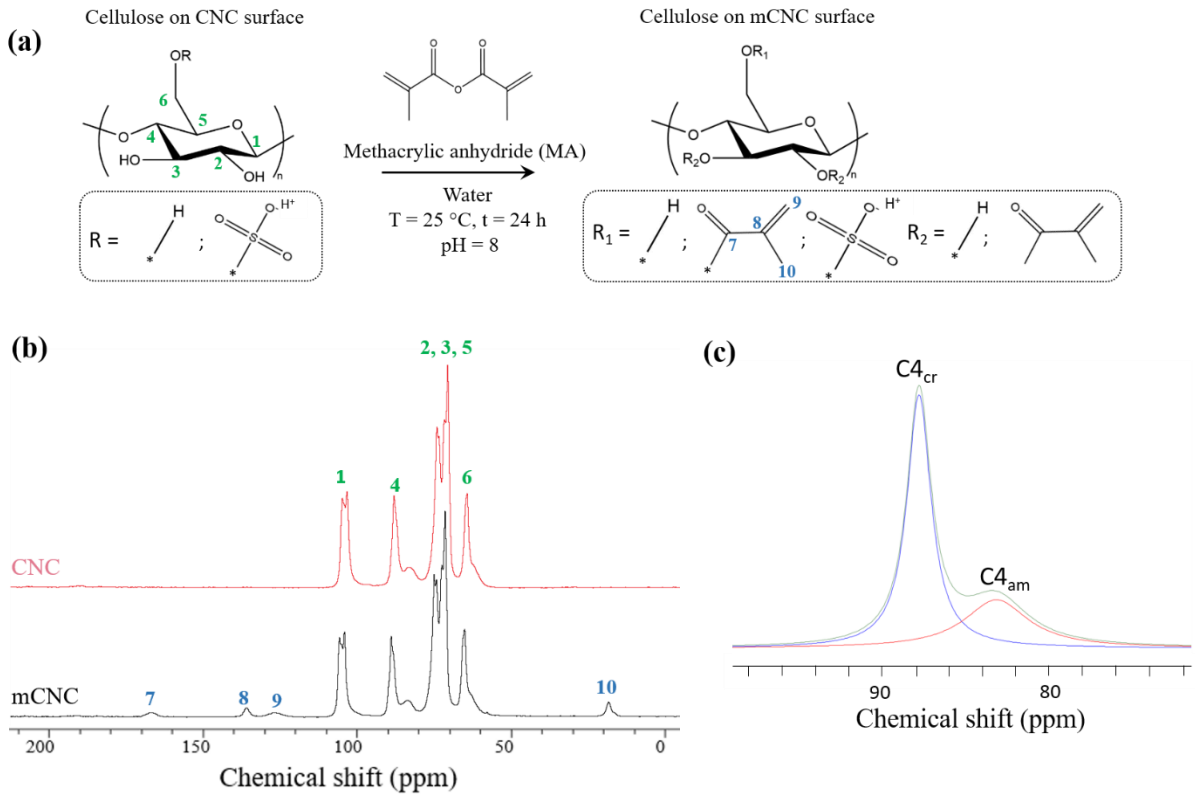

Figure 1. (a) Scheme of the methacrylation of CNCs with methacrylic anhydride (MA) in water at 25 °C to yield mCNCs. Since the reaction only occurs on the surface, and there are no conditions for swelling or cutting chains, R1 and R2 cannot be both methacrylate groups on the same anhydroglucose unit. **(b)** ^{13}C CP-MAS solid state NMR spectra measured for the as-prepared CNCs (red) and for the mCNCs (black) obtained after methacrylation with 24 equivalents of MA per CNC surface hydroxyl groups. **(c)** Deconvolution performed on CNC C4 carbon, between 74 and 94 ppm, for the quantification of C4 crystalline ($C4_{cr}$) and amorphous ($C4_{am}$) phases.

The influence of the $N_{MA}/N_{OH(surf)}$ molar ratio on the final DM of mCNCs was studied. By increasing $N_{MA}/N_{OH(surf)}$ from 0 to 24, a continuous increase in the integrals of all methacrylate peaks (C7-10) was observed, leading to a linear increase in the DM (Figure 2a; $R^2 = 0.99$). A maximum DM value of 12.6 ± 0.50 % was obtained for mCNCs prepared using a $N_{MA}/N_{OH(surf)}$ ratio of 24. Based on the values of DM, a reaction efficiency equal to 1.5, 2.4, 2.3 and 1.9 %

was calculated for $N_{MA}/N_{OH(surf)}$ equal to 3, 6, 12 and 24, respectively. According to these results and since no plateau value was reached, it is quite likely that higher DM could be reached by using even higher initial $N_{MA}/N_{OH(surf)}$ ratio. It is expected that the methacrylation should preferentially be carried out on the primary hydroxyl groups of C6, which are more reactive and accessible than secondary hydroxyls. Once all the C6 hydroxyls are consumed, esterification should continue on the secondary alcohols. As a comparison with CNFs, Kelly et al.[44] only obtained a maximum of 0.07 methacrylate group per anhydroglucose (DM = 7 %) after methacrylation with MA in aqueous medium, whereas Brusentsev *et al.*[10] obtained a DM = 2 % in DMF. The only example of the application of such a methacrylation protocol to CNCs was reported by Ma et al.[45] Unfortunately, the authors did not provide any information about the obtained DM. Using 4-dimethylaminopyridine (DMAP) in dimethyl sulfoxide (DMSO), Bai et al.[41] obtained a low DM of 0.68 %. Using a series of organic solvents for the reaction and purification steps (DMF, pyridine, toluene and acetone) and a large excess or MA for the methacrylation of CNCs, Siqueira and coworkers reached DM values comparable to those in the present work. Overall, these comparisons with literature data evidence that our aqueous medium protocol enables us to achieve DM values greater than or equal to those reported in the literature with the use of organic solvents. Furthermore, even if the use of organic solvents prevents the hydrolysis of MA, it seems that large excess of MA are still required to reach DM values similar to ours.

Interestingly, the methacrylation of CNCs seemed to lower their dispersibility in water. Indeed, the obtained mCNCs were not or poorly dispersed (Supporting Information Figure S3a,b) in water as aggregation and sedimentation effects were observed. Nanocrystal dispersion in water is possible thanks to the electrostatic repulsions between sulfate half-ester groups on the CNC surface that are covalently grafted during hydrolysis.[46] First, methacrylates are hydrophobic moieties and their grafting on the surface of the CNCs is expected to increase the CNC

hydrophobicity. Second, methacrylation might affect the amount of sulfate groups on the CNC surface. In this context, conductometric titration was used to determine the surface sulfate half-ester content of as-prepared and methacrylated CNCs samples (Supporting Information Figure S4). Non-modified CNCs had a degree of sulfation (DS) of 3.34 ± 0.21 %. After methacrylation, the DS decreased progressively when increasing the $N_{MA}/N_{OH(surf)}$ molar ratio (Figure 2a). As an example, for MA/OH_{surf} ratios of 3.0 and 24, a loss of 35 % (DS = 2.06 ± 0.07 %) and 77 % of the sulfate content (DS = 0.78 ± 0.03 %) was respectively noticed. It has been shown that the addition of NaOH could lead to desulfation of the CNCs.[60,61] Kloser and Gray [62] added 1.7 M NaOH at 85 °C during 72 h to a 2.8 wt% CNC dispersion and observed a decrease of 83 % of the sulfate content. To verify the impact of NaOH addition on the DS and hence on the nanocrystal suspension stability during the methacrylation process, 0.05 M NaOH was added to 100 mL of a 2.3 wt% CNC water dispersion until pH = 10 and let during 24 h under stirring. After purification, the final DS was 1.80 ± 0.07 %, i.e. 47 % lower than the initial DS. In our methacrylation experiments, the higher the $N_{MA}/N_{OH(surf)}$ ratio, the larger the needed volume of NaOH to complete the reaction. Such an increase in the NaOH content thus explains the concomitant decrease in DS and increase in DM.

To understand how DM and DS evolved during the reaction, a kinetic study was performed during the CNC methacrylation using a $N_{MA}/N_{OH(surf)}$ ratio of 12 (Figure 2b). A maximum DM of 6.3 ± 0.34 % was reached when the reaction was stopped after 24 h. The DM rapidly increased during the first 2 h and then the methacrylation kinetic decreased. As a result, the amount of NaOH added to keep the pH at 8 was reduced. Similarly, the DS decreased rapidly in the first 2 h (32 %) and then more slowly up to 24 h. This evolution of DS was explained by the amount of NaOH added over time. To avoid the loss of sulfates and the consequent detrimental effect on the colloidal stability of mCNCs in water, the grafting of carboxylates on the CNC surface, for example through TEMPO-mediated oxidation, could be envisioned.[10,63]

However, we rather made the choice to make a compromise between DM and DS values by choosing conditions when DS was still high enough to ensure colloidal stability and DM was high enough to enable efficient crosslinking. Accordingly, a 30 min reaction using a $N_{MA}/N_{OH(surf)}$ of 3.0 yielding mCNC with a DM of 0.83 ± 0.040 % and a DS of 2.9 % was selected. The obtained mCNC dispersion did not sediment (Supporting Information Figure S3c), and was further used in the rest of the study. The DM value of 0.83 % corresponds to a surface degree of methacrylation (DM_{surf}) of 2.3 % calculated with equation 5:

$$DM_{surf}(\%) = \frac{DM}{0.32} \quad (5)$$

where 0.32 is the number of surface chains in the structure of CNCs from cotton determined by ^{13}C CP-MAS solid-state NMR, and only half of the hydroxyl groups are accessible on the surface.[47] The maximum DM of 12.6 % obtained with $N_{MA}/N_{OH(surf)}$ = 24 indicates a DM_{surf} of 39 %, i.e. 26 % of surface hydroxyl groups.

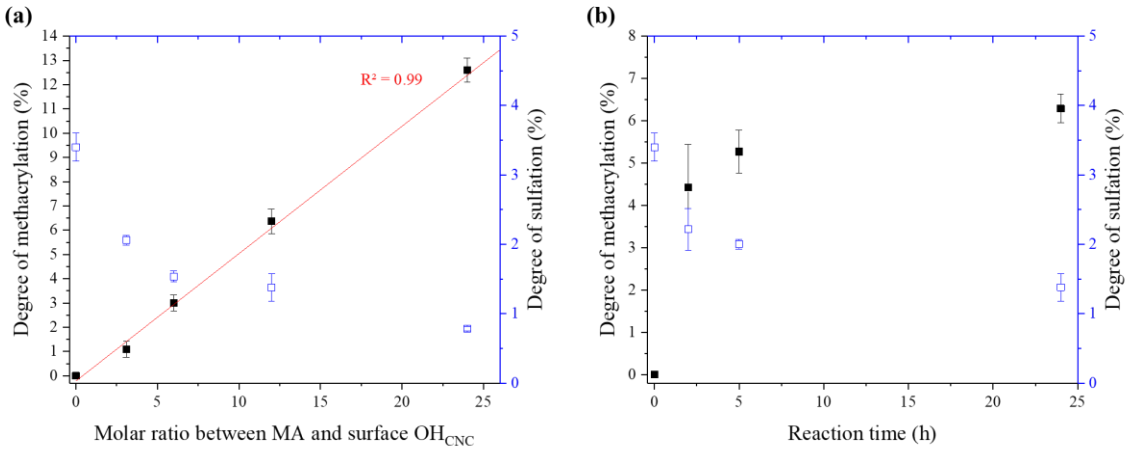

Figure 2. Evolution of the degrees of methacrylation (DM) and sulfation (DS) of methacrylated mCNCs with **(a)** the molar ratio $N_{MA}/N_{OH(surf)}$ between methacrylic anhydride (MA) and CNC surface hydroxyls (OH_{CNC}) after 24 h of reaction and **(b)** with the reaction time using a $N_{MA}/N_{OH(surf)}$ of 12. DS and DM values were measured by conductometric titration and NMR spectroscopy, respectively. Error bars depend on the C10 carbons integration processing of the

NMR spectra from two different reactions. For DS, error bars depend on the number of DS measurements [2-3].

Before addition in mCMC formulations, the dispersions of mCNC with a DM of 0.83 % were characterized by TEM and DLS. TEM images showed no difference in the morphological characteristics of the nanoobjects before and after methacrylation (Supporting Information Figure S5). Individualized nanocrystals made of a few laterally aggregated elementary crystallites were observed in both dispersions. All the individual cellulose nanocrystals displayed a length inferior to 200 nm, in good agreement with the literature.[48] DLS measurements revealed in both cases a monomodal size distribution centered around a hydrodynamic diameter of 98 nm and 91 nm for the CNC and the mCNC dispersions, respectively, and no aggregates were observed (Supporting Information Figure S6.). Therefore, TEM and DLS results show that the selected mCNC sample exhibits a comparable morphology and colloidal stability in water as the as-prepared CNCs.

3.2. Influence of the concentration and methacrylation of CNCs on the rheological and optical properties of photo-crosslinkable mCMC formulations.

Based on our previous study concerning CMC formulations, a photo-crosslinkable formulation composed of 2 wt% mCMC with a DM of 0.34 (mCMC-34) was selected as a reference for its low viscosity (Formulation F_0, Table 1).[16] Indeed, at 1 s^{-1} and 25 °C, the viscosity of this solution was only of 20.0 ± 7.0 mPa.s. CNCs and mCNCs were then added at two different concentrations (0.2 or 0.5 wt%) in the reference formulation to study their influence on the properties of hydrogels obtained after UV-curing (Table 1).

Table 1. Composition of the photo-crosslinkable mCMC formulations containing 0 to 0.5 wt% of as-prepared methacrylated CNCs.

Formulation		mCMC-34 concentration (wt%)	CNC concentration (wt%)	mCNC concentration (wt%)	Irgacure 2959 concentration (wt%)[a]
	DS	-	3.4 %	2.9 %	
	DM	0.34	-	0.83%	
F_0		2	-	-	0.12
$FCNC_{0.2}$		2	0.2	-	0.12
$FCNC_{0.5}$		2	0.5	-	0.12
$FmCNC_{0.2}$		2	-	0.2	0.13
$FmCNC_{0.5}$		2	-	0.5	0.14

[a] The mass percentage of Irgacure 2959 was determined relatively to the total methacrylate concentration in each formulation.

For 3D printing, the process parameters usually depend on the viscosity of the formulations.[64] Therefore, the shear viscosity of all CNC- and mCNC-containing formulations was measured. Each formulation displayed a shear-thinning behavior (Figure 3a). The addition of CNC or mCNC increased the viscosity of the formulations over the entire frequency range (0.1 - 100 s^{-1}), as already observed by Hassan et al.[65] and Fonsêca and d'Ávila[66] with the incorporation of CNCs in CMC solutions. As an example, at 1 s^{-1}, the reference formulation, F_0, had a viscosity of 20.0 ± 7.0 mPa.s, whereas formulations $FCNC_{0.5}$ and $FmCNC_{0.5}$, containing respectively 0.5 wt% of CNCs or mCNCs, presented a viscosity of 280 ± 66 mPa.s and 1600 ± 390 mPa.s, respectively. The formulation viscosity also increased with the concentration of CNCs or mCNCs. At 1 s^{-1}, the formulation viscosity was for example 86.0 ± 3.7 mPa.s with 0.2 wt%

CNC, and 280 ± 66 Pa.s with 0.5 wt% CNC. Moreover, the formulations containing mCNCs displayed a higher viscosity than those with CNCs, probably because of more complex interactions between mCNCs and mCMC. Indeed, several types of interactions could be involved in these formulations. First, van der Waals interactions and hydrogen bonding between mCMC and CNC or mCNC could occur, even in the presence of negative charges brought by carboxylate groups on the mCMC backbone.[34,67,68] The lower surface sulfate content of mCNCs could probably facilitate the surface absorption of mCMC onto the nanorods. Due to the presence of methacrylate groups on both mCMC and mCNC, hydrophobic interactions between these two compounds could also occur, increasing the possibility of mCMC adsorption on mCNCs. Interactions between the CMC chains adsorbed on the mCNC could create a network structure, which would hinder the movement of the particles in the suspension, resulting in an increase in the viscosity of the suspension compared to that containing CNCs, where this phenomenon would be lowered. Finally, CNCs or mCNCs repel each other by electrostatic repulsions due to the presence of sulfate groups. Consequently, the destructuration of the material interactions under shear, as well as the orientation of the nanorods, could probably explain the shear-thinning properties of all studied formulations. Furthermore, the differences in viscosity between the different formulations were significantly large, which requires the photo-crosslinking parameters (UV irradiance, insolation time, etc.) to be adjusted specifically for each formulation.

Limiting the scattering of the UV beam in the z-direction in the formulation during printing is important, as it is a way to enhance the process resolution.[69]. UV-vis absorption is an essential characteristic that defines the ability of a compound to limit light penetration. Therefore, the absorbance spectra of CNC and mCNC suspensions in water and in a mCMC solution were measured. Interestingly, CNC dispersions displayed higher absorbance for the same concentration in water than mCNC dispersions, irrespective of the wavelength in the probed

range (Supporting Information Figure S7). Moreover, for both types of nanocrystals, UV-vis absorbance increased by increasing the concentration of nanorods. The incorporation of CNCs and mCNCs into mCMC solutions induced a significant increase in the absorbance (Figure 3b). The formulation absorbance also increased with the concentration of CNCs and mCNCs. Contrary to aqueous suspensions, the absorbance of mCNC formulations was higher than that of CNC formulations. Even if the role of the interactions between the components on the UV-vis absorption is difficult to assess, the observed increase in absorbance was probably not provided by the addition of methacrylates from the mCNC since the latter absorbed below 250 nm[70] and no absorbance was observed for the formulation F_0 that contained methacrylate groups. At the specific photo-crosslinking wavelength of 365 nm, mCNC-containing formulations showed a more important absorption than CNC-containing samples (A_{365} (F_0) = 0.095, A_{365} ($FCNC_{0.5}$) = 1.99 and A_{365} ($FmCNC_{0.5}$) = 2.61). As for the viscosity, these differences of absorbance between formulations could also induce some adjustments in the photo-crosslinking parameters.

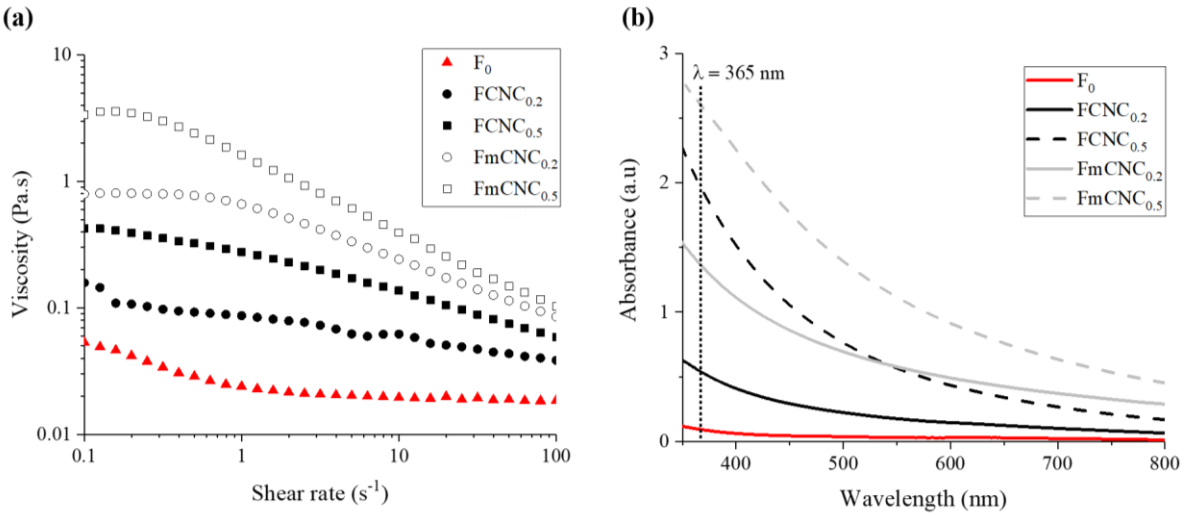

Figure 3. (a) Viscosity flow curves measured from 0.1 to 100 s^{-1} at 25 °C for the reference (F_0) and for CNC ($FCNC_{0.2}$ and $FCNC_{0.5}$) and mCNC-containing ($FmCNC_{0.2}$ and $FmCNC_{0.5}$) formulations. **(b)** UV-vis spectra for the five formulations before the introduction of the

photoinitiator. The relevant absorbance for 3D printing lies in the UVA part at λ = 365 nm (dashed vertical line)

3.3. Photocrosslinking of formulations. The photo-crosslinking kinetics of all formulations were characterized by RT-rheology in order to provide essential information about the needed insolation time using vat polymerization techniques. Before irradiation, all formulations presented a viscous liquid behavior, with a loss modulus, G", higher than the storage modulus, G' (Supporting Information Figure S8). Photo-crosslinking of methacrylates started with the application of UV light and led to a progressive increase of the G' and G" values until reaching a solid-like behavior (G' > G"). The gelation time (t_{gel}) was then determined at the intersection between G' and G" curves. It is well established for UV-curable resins used in vat polymerization techniques that the insolation time for each layer must be at least equal to t_{gel} in order for the layer to be rigid enough to be self-standing.[71] After the gelation, both shear moduli continued to increase with UV exposure until reaching a plateau corresponding to the maximum conversion of methacrylates under the oscillation conditions used.

Contrary to previous results from Cafiso et al.,[36] the integration of CNCs did not significantly reduce the crosslinking rate of mCMC (Figure 4). Indeed, gelation times of 22 ± 1.0 s, 20 ± 0.90 s and 19 ± 1.1 s were respectively measured for formulations F_0, $FCNC_{0.2}$ and $FCNC_{0.5}$. Interestingly, the integration of mCNC significantly speeds up the photo-crosslinking kinetics of mCMC formulations. Indeed, gelation times of 16 ± 1.2 s and 9.6 ± 1.5 s were measured for formulations containing 0.2 wt% ($FmCNC_{0.2}$) and 0.5 wt% of mCMC ($FmCNC_{0.5}$), respectively. One could explain this phenomenon by the presence of methacrylate groups on the mCNC surface that participate in the crosslinked network. These results clearly demonstrate the potential of mCNC addition in photo-crosslinkable and 3D-printable formulations for reducing the printing time. These results are in good agreement with the gel

time value of 30 s recently reported by Brusentsev et al. for a 1.1 wt% methacrylated cellulose nanofibrils (DS = 2%), 1% acrylamide and 0.4 wt% Irgacure 2959 formulation.[10]

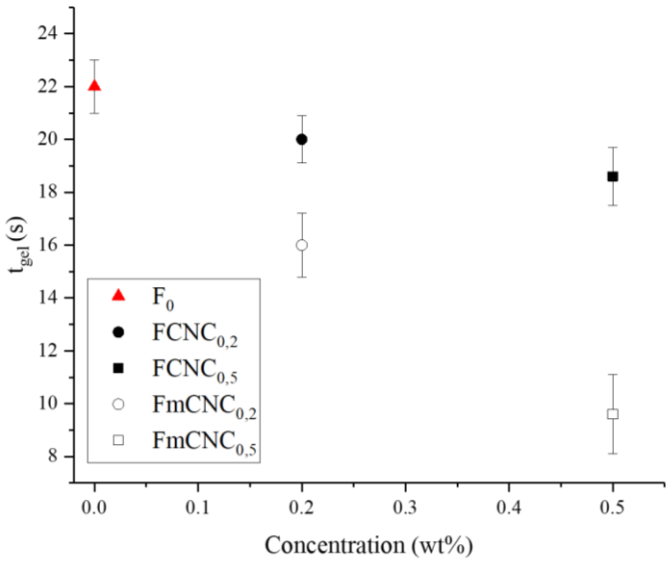

Figure 4. Gelation time (t_{gel}) measured by RT-rheology for photo-crosslinkable mCMC formulations containing CNCs or mCNCs at a concentration from 0 to 0.5 wt%. Error bars are standard deviations from three different measurements per formulation.

In agreement with their increased UV absorbance at 365 nm, mCNC-containing formulations offered both reduced printing time and increased resolution in the three space directions (x,y,z), resulting in a more accurate design of the printed objects (Figure 5a). This was proven by measuring the depth in the z-direction of the crosslinked layer for different formulations, as a function of exposure time under UV light (Figure 5b). For all the considered formulations, the hydrogel structure was too weak after an exposure time equal to t_{gel}, and no thickness measurement could be done with our experimental procedure. However, the lower the t_{gel}, the faster a mechanically stable hydrogel was obtained. Indeed, an exposure time of 32 s was required to obtain easy-to-handle hydrogels from the reference formulation (F_0), while exposure times of only 25 s and 15 s were needed for the formulations containing 0.5 wt% of raw CNC ($FCNC_{0.5}$) and mCNC ($FmCNC_{0.5}$), respectively. Interestingly, the crosslinked hydrogel

thickness for all formulations increased linearly with the irradiation time ($R^2 > 0.98$). Finally, for the same exposure time, the thickness of the hydrogel clearly depends on the presence of CNC or mCNC in the formulation, even if no significant difference was observed between the two types of particles. For example, at 60 s, the hydrogels displayed a crosslinked thickness of respectively 5.2 ± 0.3 mm and 4.9 ± 0.3 mm, when issued from $FmCNC_{0.5}$, and $FmCNC_{0.5}$, respectively, whereas a thickness of 6.9 ± 0.3 mm was obtained from F_0. Consequently, the presence of CNC or mCNC clearly reduced the crosslinking and led to a lower z-layer thickness in a shorter time than for the reference mCMC formulation.

A slight increase in the hydrogel diameter, corresponding to x and y directions, was observed for irradiation times higher than 30 s in the presence of CNCs or mCNCs (Supporting Information Figure S9) as observed by Cafiso et al.[36] However, it has to be noted that negligible particle scattering and good in-plane dimensional control are achieved by keeping the UV irradiation time below 30s. Overall, formulations containing CNCs or mCNCs allowed achieving better resolutions in all three spatial directions (x, y, z), as shown by the more precise design of the cross-linked hydrogels illustrated in Figure 5b. This result could primarily be linked to the greater stiffness induced by the presence of CNCs and mCNCs, in contrast to F0 after 45 s of exposure. In addition, the cross-linking rate is higher with mCNCs than with CNCs, which explains the better resolution achieved with mCNCs.

An increase in the hydrogel diameter, corresponding to x and y directions, was observed for irradiation times higher than 30 s in the presence of CNCs or mCNCs (Supporting Information Figure S9) as observed by Cafiso et al.[36] However, it has to be noted that negligible particle scattering and good in-plane dimensional control are achieved by keeping the UV irradiation time below 30s. Overall, formulations containing CNCs or mCNCs allowed achieving better resolutions in all three spatial directions (x, y, z), as shown by the more precise design of the cross-linked hydrogels illustrated in figure 5a. This result could primarily be linked to the

greater stiffness induced by the presence of CNCs and mCNCs, in contrast to F0 after 45 s of exposure. In addition, the cross-linking rate is higher with mCNC than with CNC, which explains the better star resolution achieved with mCNC. Finally, after freeze-drying, the shape and dimensions of the cryogels remained the same as that of the starting hydrogels.

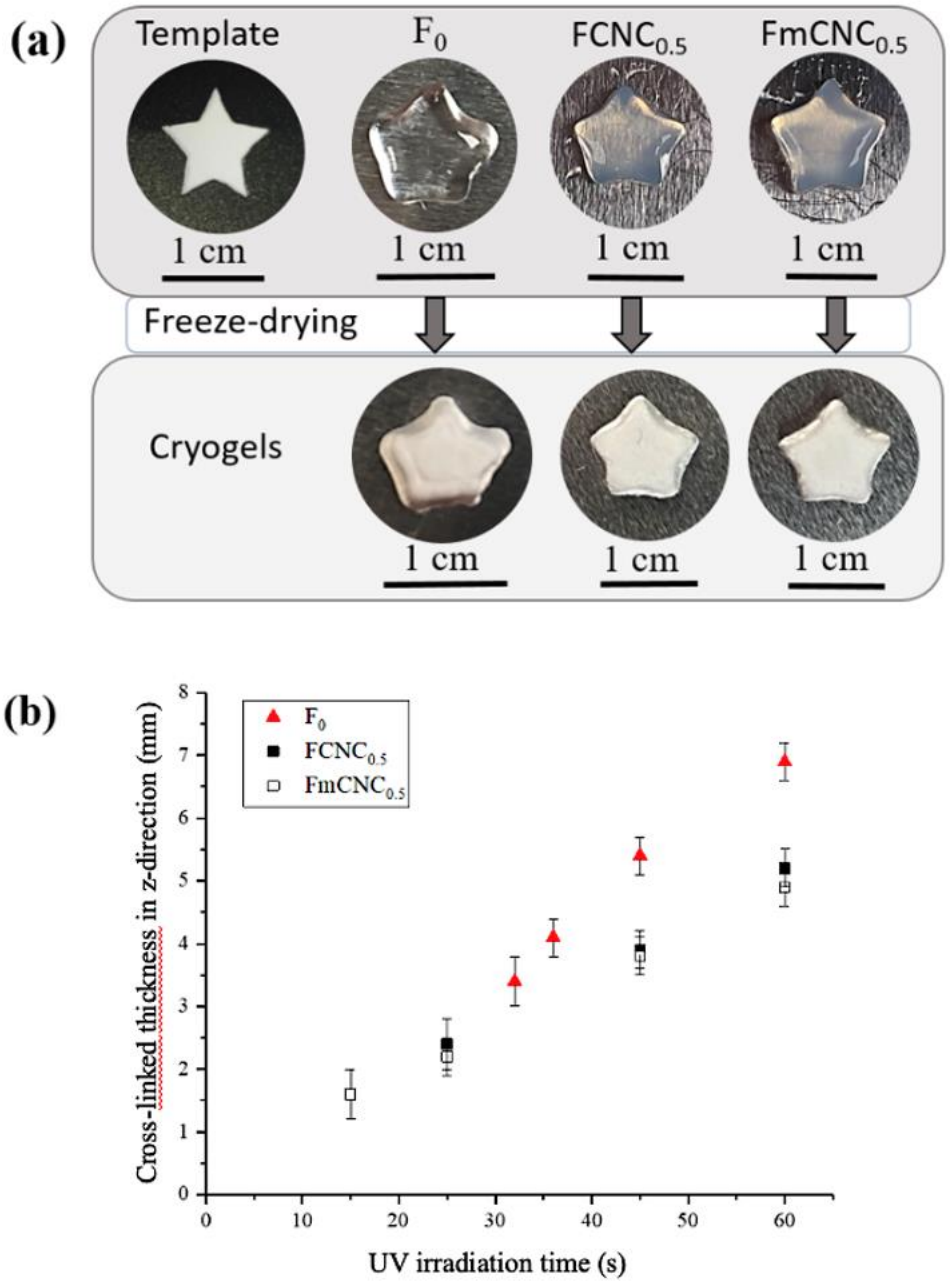

Figure 5. (a) Illustration of the influence of the integration of 0.5 wt% of CNC or mCNC in the photo-crosslinkable mCMC formulations on the x- and y-resolutions of hydrogels obtained after a 45 s exposure under UV light, and of the corresponding cryogels obtained by freeze-

drying. **(b)** Evolution of the thickness of the photo-crosslinked hydrogel (z-direction) as a function of the exposure time under UV light (365 nm) for the reference formulation (F_0), and for formulations containing 0.5 wt% CNCs ($FCNC_{0.5}$) or mCMCs ($FmCNC_{0.5}$). Error bars depend on the number of measurements performed at different locations of the crosslinked hydrogels.

3.4. Characterizations of hydrogels. A UV post-curing was then applied to the photo-crosslinked hydrogels to reach the maximum conversion of methacrylate groups and to reinforce the hydrogel structure. The methacrylate conversion ratio (CR), corresponding to the percentage of crosslinked methacrylate over the total number of methacrylate groups, and the exposure time necessary to achieve the maximum CR were determined by ^{13}C CP-MAS NMR spectroscopy on freeze-dried cryogels (Supporting Information Figure S10). The influence of the UV insolation duration was investigated in our previous work.[16] Based on these results, the photo-crosslinking reaction was considered completed after 5 min and this time was selected for the subsequently-described experiments.

The CR of cryogels obtained after 5 minutes of exposure were calculated for each formulation (Table 2). First, the integration of non-methacrylated CNCs decreased the CR, since they did not participate in the crosslinking and their presence certainly restricted the mobility of mCMC chains. In contrast, the CR increased with the integration of mCNCs since they are able to participate in crosslinking thanks to the methacrylate groups on their surface. From these CR values, and as the volume of both the hydrogels and cryogels was constant (0.64 cm^3), crosslinked methacrylate group densities of 3.2 to 4.9 µmol/cm^3 were calculated for these materials (Table 2). Obviously, the same evolution as with the crosslinking ratio was observed with CNC integration in the mCMC formulation and with their concentration (Table 2, Figure 6a). In their work, Cafiso et al.[36] showed that the crosslinked methacrylate density increased with the addition of either CNC or mCNC by considering the G' modulus value obtained at the

plateau of RT-rheology measurements. The increase in crosslinked methacrylate density with mCNC was explained by their covalent participation in the network. However, no explanation was provided for the increase in crosslinked density with the addition of CNC, as the latter are unable to participate in the network.

Moreover, considering the volume of both the hydrogels and cryogels and the number of methacrylate groups as constant, a lower CR value induces a higher ratio of free methacrylate functions in the material (Figure 6b). The presence of methacrylate groups could be an undesirable cause of cytotoxicity[72], and should consequently be avoided in biomaterials. The free methacrylate group density increased with the addition of CNCs, as well as with increasing their concentration. On the contrary, it decreased with the addition of mCNCs, since more methacrylates were consumed in crosslinks (Table 2).

Water swelling ratios (SR) reflecting the capacity of hydrogels to absorb and retain water without breaking were measured. For all considered hydrogels, swelling equilibrium was achieved in less than 10 hours (Supporting Information Figure S11). Interestingly, the swelling ratio decreased with the presence of CNCs or mCNCs and this effect was reinforced at higher concentrations (Table 2). The SR value was lower in the presence of mCNCs compared to the reference without nanocrystals (F_0), due to the higher crosslinked methacrylate density, making the network more resistant to expansion. In the case of CNC addition, the density of crosslinked methacrylates was lower than that of F_0, resulting in a higher quantity of free methacrylates. This excess of free methacrylate groups exhibiting hydrophobic characteristics could hinder water absorption into the network (Table IV-2). Ultimately, the slight difference in swelling between hydrogels containing CNCs or mCNCs at equivalent concentrations could arise from a combined effect of reduced swelling due to increased crosslinking density and decreased swelling caused by the increase in free methacrylates.

Table 2. Structural properties of photo-crosslinked hydrogels obtained after 5 minutes insolation and of the corresponding freeze-dried cryogels.

Formulation	Conversion of methacrylates (CR, %)	Crosslinked methacrylate density (µmol/cm^3)	Free methacrylate density (µmol/cm^3)	Hydrogel swelling ratio at equilibrium (SR)
F_0	53 ± 2	4.3 ± 0.29	3.8 ± 0.20	3.4 ± 0.14
$FCNC_{0.2}$	43 ± 2	3.5 ± 0.15	4.6 ± 0.24	3.2 ± 0.070
$FCNC_{0.5}$	40 ± 2	3.2 ± 0.13	4.8 ± 0.19	3.0 ± 0.19
$FmCNC_{0.2}$	55 ± 2	4.5 ± 0.25	3.7 ± 0.25	3.1 ± 0.12
$FmCNC_{0.5}$	58 ± 2	4.9 ± 0.29	3.6 ± 0.26	2.8 ± 0.12

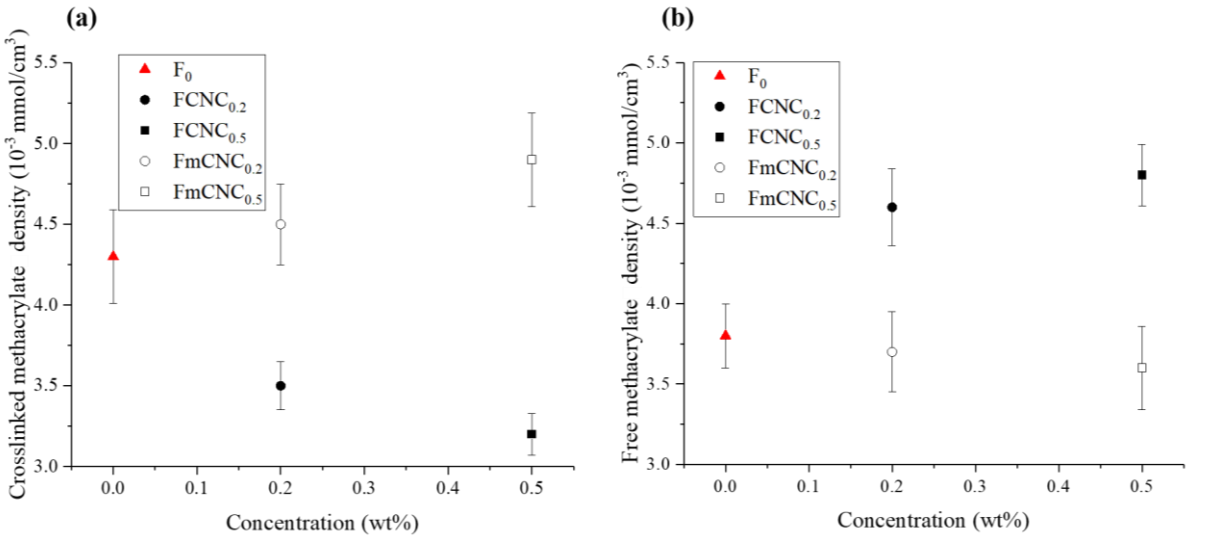

Figure 6. Influence of the concentration of as-prepared CNCs or methacrylated CNCs in photo-crosslinkable mCMC formulations on the densities of crosslinked methacrylates **(a)** and of free methacrylates **(b)** in photo-crosslinked hydrogels, estimated from the methacrylate conversion rate (CR) measured by NMR spectroscopy.

The impact of the crosslinked methacrylate density on the hydrogel mechanical properties was investigated by rheology. Frequency oscillation measurements at 1% strain and at 25 °C allowed us to determine the elastic modulus, G', the viscous modulus, G'', and the loss factor $\tan(\delta) = \frac{G''}{G'}$, where δ is the phase shift and is characteristic of the viscoelastic properties of the material, of all hydrogels (Figure 7, Supporting Information Figure S12). It is worth remembering that tan(δ) values superior to 1 mean that the material is viscous. Conversely, a value close to 0 indicates that the material has solid elastic characteristics. For the considered hydrogels, tan(δ) values decreased with the addition of CNCs and mCNCs, due to the mechanical reinforcement of the hydrogel structure (Figure 7a). Indeed, at 1 Hz, average tan(δ) values of 0.016 ± 0.0088 and 0.025 ± 0.0054 were respectively measured for the hydrogels obtained from the mCMC formulations containing 0.5 wt% CNC ($FCNC_{0.5}$) or 0.5 wt% mCNC ($FmCNC_{0.5}$). Thes values are much lower than the tan(δ) value 0.054 ± 0.0033 measured for the reference hydrogel, F_0. However, no significant tan(δ) variation was observed when comparing the addition of CNCs or mCNCs and upon concentration variations. As an example, average tan(δ) values of 0.016 ± 0.0014 and 0.016 ± 0.0088 were obtained for the hydrogels containing 0.2 wt% CNC ($FCNC_{0.2}$) and 0.5 wt% mCNC ($FCNC_{0.5}$), respectively. All these tan(δ) values were very close to 0, indicating that all the hydrogels exhibit a solid behavior on the considered frequency range. As a matter of fact, the nanocrystals took up additional space in the matrix, increasing the cellulosic material mass (Table S1). A higher material density leads to stronger interactions, resulting in an increase in the elasticity of the hydrogel. Moreover, it has been shown in our previous work on pure mCMC hydrogels that the concentration was the most essential parameter to explain the variations in the viscoelastic properties.[16] However, it might not be the only influencing parameter as no significant difference of tan(δ) values was measured between hydrogels containing different CNC and mCNC concentrations. This could be explained by a potential inhomogeneity in the dispersion of cellulose nanocrystals in the

hydrogel as the concentration increases, modifying the organization of the crosslinked network. As a result, the hydrogel mechanical properties were impacted, limiting the continuous improvement of hydrogel elasticity observed by Yang et al.[72] on poly(ethylene glycol)-based hydrogels reinforced with CNCs. Finally, the strengthening effect of CNCs and mCNCs in the hydrogel structure on the elastic modulus G' can be demonstrated. Indeed, the latter increases with the addition of modified or unmodified nanocrystals. For example, at 1 Hz, the elastic modulus G' is 1362 ± 55 for the F0 formulation, whereas it is 1903 ± 331 or 1923 ± 227 when 0.5 wt% CNCs or mCNCs are respectively incorporated (Supporting Information Figure S12). Comparable values for the elastic modulus G' with the same concentration of CNCs or mCNCs seem to indicate that the reinforcement phenomenon associated with the presence of the fillers is more important than the crosslinking density, which increases with the presence of mCNCs.

The rheological study was also conducted on swollen hydrogels at equilibrium, after 24 h in deionized water at room temperature (Supporting Information Figure S13, Figure 7b). As expected, swollen hydrogels displayed a higher tan(δ) over the entire frequency range than the original hydrogels since they contain more water (Figure 7b). However, the ranking of the swollen hydrogels was different than that of the initial hydrogels. Indeed, at 1 Hz, equivalent average tan(δ) values of 0.61 ± 0.055, 0.64 ± 0.10 and 0.56 ± 0.094 were measured for the swollen hydrogels obtained from the reference formulation F_0, and from the formulations containing 0.2 wt% CNC ($FCNC_{0.2}$) and 0.5 wt% CNC ($FCNC_{0.5}$), respectively. The average tan(δ) value for the swollen hydrogels with and without CNCs indicated equivalent viscoelasticity properties. In contrast, hydrogels containing mCNC showed tan(δ) values at least two times lower than the CNC-containing hydrogels. This difference was explained by the release of CNCs into the water bath during the swelling of hydrogels derived from formulations $FCNC_{0.2}$ and $FCNC_{0.5}$, which was highlighted by measuring the mass variation of the swollen

hydrogels after drying (Supporting Information Table S1). In contrast, mCNC were covalently crosslinked to the mCMC network and could not be released. They consequently contributed to the stiffness of the swollen hydrogel. Finally, the addition of 0.5 wt% mCNC in the formulation allowed for preserving interesting elastic properties while limiting the hydrogel swelling, which is desirable for certain applications such as soft tissue engineering. [74]

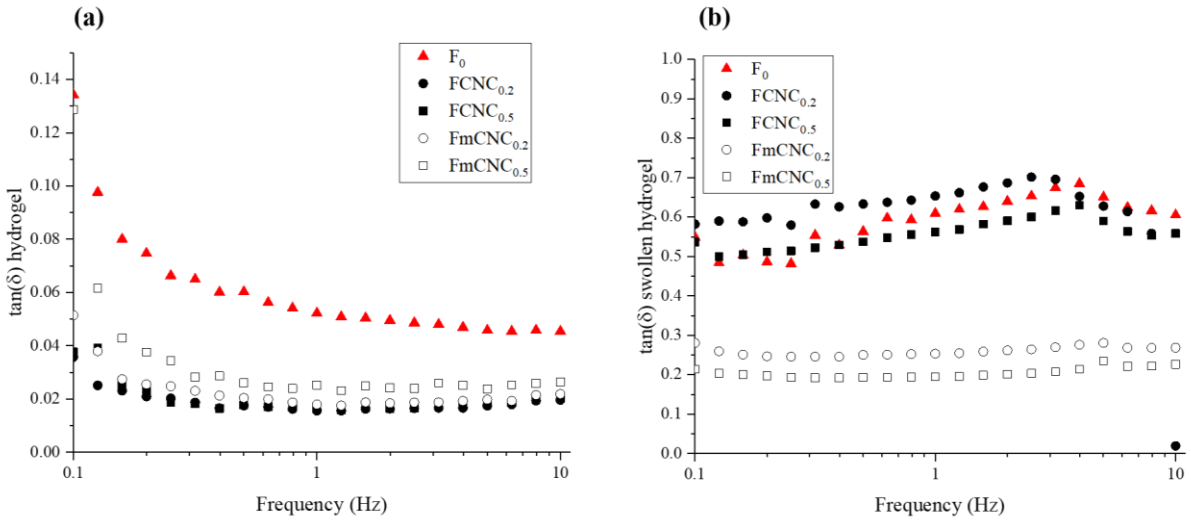

Figure 7. Evolution of the loss factor (tan(δ)) of the photo-crosslinked hydrogels before **(a)** and after swelling **(b)**, measured by parallel plate rheology, between 0.1 and 10 Hz, at 1 % strain and at 25 °C. All the points correspond to an average of three different values obtained from three different samples.

3.5. Cytotoxicity investigation. Prior to cell seeding, all the cryogels were sterilized and stored into a culture medium until used. The visual inspection of the samples revealed a pinkish appearance due to the intrinsic color of the culture medium (Figure 8a). In parallel, their labelling with ethidium homodimer-1 (during the Live/Dead® assay) revealed an unexpected but very helpful red fluorescence enabling the observation of their structure (Figure 8b). In contrast to swollen CNC-free cryogels (F_0), swollen CNC- and mCNC-containing ones

(respectively $FmCNC_{0.2}$ and $FmCNC_{0.5}$) exhibited homogeneously distributed pores that were more elongated for methacrylated CNCs. As a comparison, the dry cryogel pore size was smaller (Supporting Information Figure S14) than that of hydrated cryogels (Figure 8b). For example, F_0, $FCNC_{0.5}$ and $FmCNC_{0.5}$ dried cryogels had an average pore size of 18.9 ± 6.5 µm, 14.6 ± 2.9 µm and 15.4 ± 4.6 µm, whereas the corresponding hydrated cryogel pore sizes were 22.7 ± 6.6 µm, 22.5 ± 6.8 µm and 28.9 ± 7.6 µm, respectively (Supporting Information Figure S15). This could be explained by the material hydration and thus an enlargement of the pores induced by network swelling (Supporting Information Figure S14, S15).

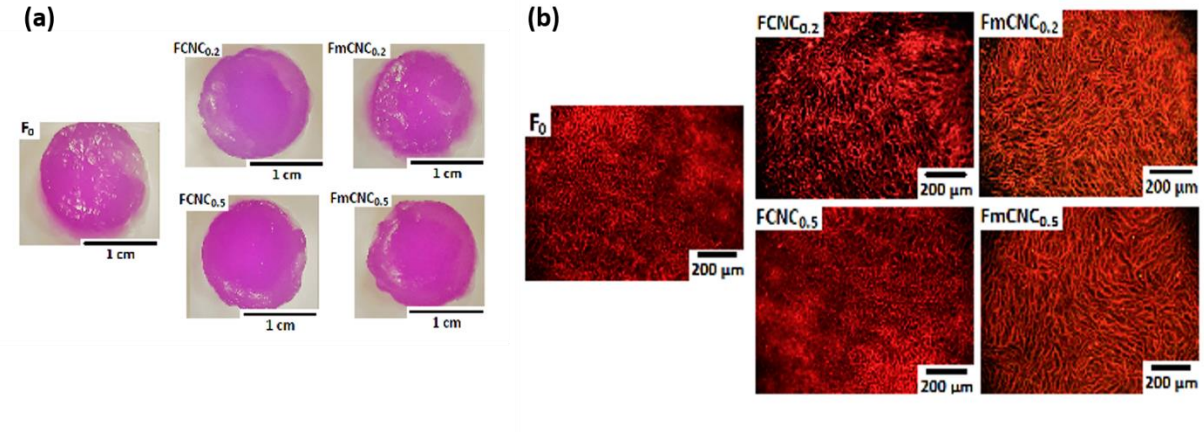

Figure 8. (a) Visual inspection of sterilized and conditioned cryogels into cell culture medium and **(b)** representative fluorescence microscopy images of cryogel porosity after labeling with ethidium homodimer-1.

Then, the cytotoxicity of the cryogels was first assessed through an *in situ* elution test to check the potential leaching of toxic compounds in the cell culture medium. Following the cell seeding, all the samples were fully immersed in the culture medium for 48 h and cells in the vicinity were observed with an inverted microscope. For each hydrated cryogel, cells exhibited a good morphology with a well-spread aspect (Figure 9a). They even proliferated at the bottom of the wells, indicating that no toxic compounds were released from the cryogels. Second, the direct contact test was conducted by plating cells on top of the samples for 48 h. Globally, the

Live/Dead assay revealed that cells were viable as they appeared green under a fluorescence microscope (Figure 9b). However, we noticed differences between the formulations, in terms of cell concentrations. While numerous rounded cells were observed on top of F_0, $FCNC_{0.2}$ and $FCNC_{0.5}$ cryogels, fewer were detected with the hydrated cryogels containing mCNCs ($FmCNC_{0.2}$ and $FmCNC_{0.5}$). These observations indicate that the presence of mCNC altered cell anchoring or their settlement in the cryogels. Various parameters could explain such a behavior (material visco-elasticity, chemical composition, surface tension, hydrophilic/hydrophobic balance…), but the subsequent composition and viscoelasticity are likely one key explanation. Moreover, both the narrow elongated shape with an average size around 25 µm of the pores and the thin thickness of the pore walls exhibited dimensions that are not compatible with cell spreading or cell invading. L929 cells have a diameter of approximately 20 µm when rounded and around 80-100 µm when spread out, which demonstrates the challenge of penetrating the network in the latter state. Finally, the metabolic activity of L929 cells contacting the cryogels confirmed that cells remained viable up to 7 days of culture (Figure 9c), although we did not observe any significant increase of cell activity over time, which is in line with the previous microscopic observations. Pore size should be increased to achieve applications such as hydrogels dedicated to extracellular matrix or scaffolds for soft tissue engineering where cell growth is required.[75,76] In this prospect, the present work shows formulations that could be printed by additive manufacturing, like vat photopolymerization, to modulate the pore size. Nonetheless, these promising cryogels could find applications in drug delivery systems.[77,78] Alternatively, to overcome the adhesion and proliferation issues, the cytotoxicity study could be done directly on hydrogels, as shown by Brusentsev *et al.* on mCNF/acrylamide hydrogels with HeLa and HDF cells.[10]

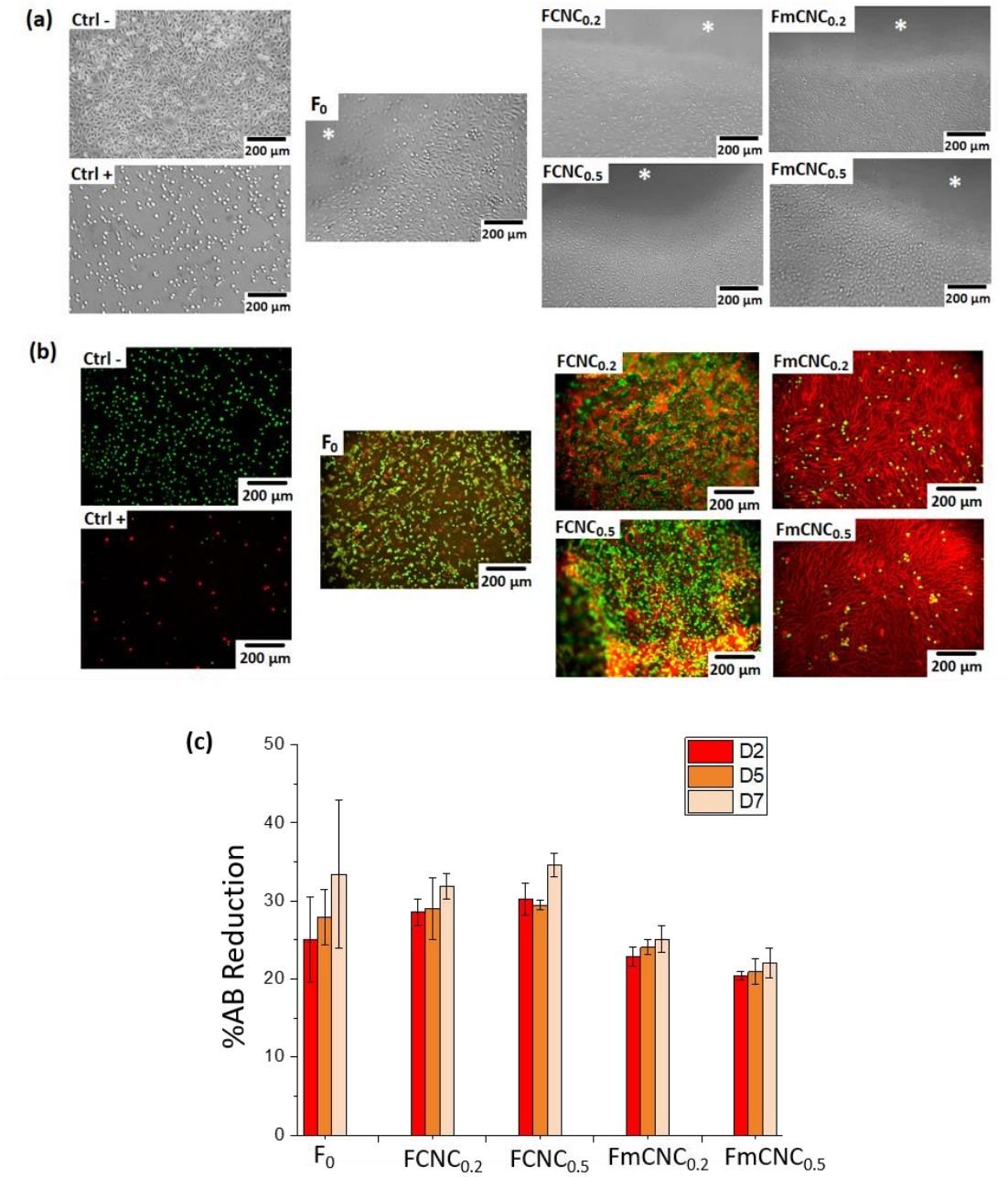

Figure 9. Cytotoxicity evaluation with L929 fibroblasts **(a)** *in situ* elution test: phase contrast inverted microscopy images of cells after 48 h of culture in the presence of cryogels (F_0, $FCNC_{0.2}$, $FCNC_{0.5}$, $FmCNC_{0.2}$ and $FmCNC_{0.5}$). Ctrl- and Ctrl+ correspond to controls (complete culture medium and 10% DMSO culture medium, respectively). * indicate the cryogel locations. **(b)** Direct contact test: epifluorescence microscopy of cells seeded on top of the cryogels for 48 h after a Live/Dead® assay. Cryogels appeared in red after ethidium homodimer-1 labelling. **(c)** Alamar Blue® assay at days D2, D5, D7.

4. CONCLUSION

In this study, aqueous cellulosic formulations were developed for the 3D printing of hydrogels by vat polymerization techniques such as stereolithography (SLA) or digital light processing (DLP). Photocrosslinkable methacrylated carboxymethylcellulose (mCMC) with a degree of methacrylation (DM) of 34 %, was solubilized in water at 2 wt% with a biocompatible photoinitiator (Irgacure 2959). Unmodified cellulose nanocrystals were added at 0.2 or 0.5 wt% in the formulation as reinforcing fillers and light scattering controllers. This addition significantly decreased the photo-crosslinking rate, the formulation crosslinked thickness (in z), and increased the rheological properties of post-cured hydrogels. However, due to CNC release, the elastic properties of swollen CNC-containing hydrogels significantly decreased after water swelling. To better improve the mechanical properties of 3D printed materials, the reaction between CNC and methacrylic anhydride (MA) was investigated to produce methacrylated cellulose nanocrystals (mCNC) able to further crosslink with mCMC. A wide range of mCNC samples with a DM between 0 and 12.6 ± 0.50 % was obtained by controlling the synthesis. However, the reaction process was detrimental to the colloidal stability of the particles in water due to the partial removal of the sulfate ester groups on the nanocrystal surface. By adjusting the protocol conditions, mCNCs with a DM of 0.83 ± 0.040 % and a sufficient sulfate amount to keep colloidal stability in water (DS = 2,9 %) were obtained. Compared to the use of CNCs, the integration of mCNCs at the same concentrations in the mCMC formulations continued to decrease the crosslinking time, the crosslinked thickness in z, while preserving the elastic properties of the hydrogel brought by the mCNC. Finally, the cryogels showed good cytocompatibility toward L929 fibroblasts. These innovative formulations could be considered for 3D printing by SLA and DLP to fabricate hydrogels or cryogels dedicated to medical applications.

ASSOCIATED CONTENT

Supporting information

The following files are available free of charge

Additional experimental details and methods; Scheme showing the protocol used for the characterization of the crosslinked hydrogel thickness; ^{13}C CP-MAS solid-state NMR spectra of mCMC (DM =34 %); Images of mCNC dispersion; Conductivity titration of CNCs; TEM images of CNCs and mCNCs; DLS measurements; UV-vis spectra of CNC and mCNC dispersions in water; RT-rheology spectra; Evolution of the diameter in x- and y-directions of photo-crosslinked hydrogels; ^{13}C CP-MAS solid-state NMR spectra of $FmCNC_{0.5}$ cryogel; Swelling ratio of hydrogels; Oscillation rheology measurements of hydrogels from different formulations; Masses of cryogels obtained from photo-crosslinked hydrogels and from swollen hydrogels; SEM images displaying the cryogel morphologies and corresponding pore size distributions.

AUTHOR INFORMATION

Corresponding Author

Bruno Jean - University Grenoble Alpes, Centre national de la recherche scientifique, Centre de recherches sur les macromolécules végétales, Saint-Martin-d'Hères, France. Email : bruno.jean@cermav.cnrs.fr

Author Contributions

All authors contributed to the study conception and design. Material preparation, data collection and analysis were performed by Lénaïc Soullard, Sébastien Rolere, Bruno Jean, Isabelle Texier, Guillaume Nonglaton, Flavie Pradalié, Béatrice Labat and Christine Lancelon-Pin. The first draft of the manuscript was written by Lénaïc Soullard and Béatrice Labat and all authors

commented on previous versions of the manuscript. All authors read and approved the final manuscript.

Funding Sources

Financial support from the cross cutting CEA program 'Matériaux et Procédés' is gratefully acknowledged (CelluloMed project). The authors acknowledge the Agence Nationale de la Recherche for financial support through the LabEx ARCANE program (ANR-11-LABX-0003-01) and the Graduate School of Chemistry, Biology and Health of University Grenoble Alpes CBH-EUR-GS (ANR-17-EURE-0003) and Glyco@Alps.

Notes

The authors have no conflicts of interest to declare.

ACKNOWLEDGMENT

The authors acknowledge the NanoBio chemistry platform (ICMG UAR 2607) for granting access to the electron microscopy facilities. The authors also acknowledge Ashland for kindly offering carboxymethylcellulose. The authors gratefully thank A. Echalard for her technical support in L929 cell culture.

REFRENCES

(1) Ngo, T. D.; Kashani, A.; Imbalzano, G.; Nguyen, K. T. Q.; Hui, D. Additive Manufacturing (3D Printing): A Review of Materials, Methods, Applications and Challenges. *Compos. Part B Eng.* **2018**, *143*, 172–196. https://doi.org/10.1016/j.compositesb.2018.02.012.

(2) Melchels, F. P. W.; Feijen, J.; Grijpma, D. W. A Review on Stereolithography and Its Applications in Biomedical Engineering. *Biomaterials* **2010**, *31* (24), 6121–6130. https://doi.org/10.1016/j.biomaterials.2010.04.050.

(3) Zhang, J.; Hu, Q.; Wang, S.; Tao, J.; Gou, M. Digital Light Processing Based Three-Dimensional Printing for Medical Applications. *Int. J. Bioprinting* **2019**, *6* (1), 1. https://doi.org/10.18063/ijb.v6i1.242.

(4) Prendergast, M. E.; Burdick, J. A. Recent Advances in Enabling Technologies in 3D Printing for Precision Medicine. *Adv. Mater.* **2020**, *32* (13), 1902516. https://doi.org/10.1002/adma.201902516.

(5) Ansari, M. A. A.; Golebiowska, A. A.; Dash, M.; Kumar, P.; Jain, P. K.; Nukavarapu, S. P.; Ramakrishna, S.; Nanda, H. S. Engineering Biomaterials to 3D-Print Scaffolds for Bone Regeneration: Practical and Theoretical Consideration. *Biomater. Sci.* **2022**, *10* (11), 2789–2816. https://doi.org/10.1039/D2BM00035K.
(6) Yourtee, D.; Emery, J.; Smith, R. E.; Hodgson, B. Stereolithographic Models of Biopolymers. *J. Mol. Graph. Model.* **2000**, *18* (1), 26–28. https://doi.org/10.1016/S1093-3263(00)00029-2.
(7) Biswas, M. C.; Jony, B.; Nandy, P. K.; Chowdhury, R. A.; Halder, S.; Kumar, D.; Ramakrishna, S.; Hassan, M.; Ahsan, M. A.; Hoque, M. E.; Imam, M. A. Recent Advancement of Biopolymers and Their Potential Biomedical Applications. *J. Polym. Environ.* **2022**, *30* (1), 51–74. https://doi.org/10.1007/s10924-021-02199-y.
(8) Mohan, D.; Teong, Z. K.; Bakir, A. N.; Sajab, M. S.; Kaco, H. Extending Cellulose-Based Polymers Application in Additive Manufacturing Technology: A Review of Recent Approaches. *Polymers* **2020**, *12* (9), 1876. https://doi.org/10.3390/polym12091876.
(9) Gauss, C.; Pickering, K. L.; Muthe, L. P. The Use of Cellulose in Bio-Derived Formulations for 3D/4D Printing: A Review. *Compos. Part C Open Access* **2021**, *4*, 100113. https://doi.org/10.1016/j.jcomc.2021.100113.
(10) Brusentsev, Y.; Yang, P.; King, A. W. T.; Cheng, F.; Cortes Ruiz, M. F.; Eriksson, J. E.; Kilpeläinen, I.; Willför, S.; Xu, C.; Wågberg, L.; Wang, X. Photocross-Linkable and Shape-Memory Biomaterial Hydrogel Based on Methacrylated Cellulose Nanofibres. *Biomacromolecules* **2023**, *24* (8), 3835–3845. https://doi.org/10.1021/acs.biomac.3c00476.
(11) Seddiqi, H.; Oliaei, E.; Honarkar, H.; Jin, J.; Geonzon, L. C.; Bacabac, R. G.; Klein-Nulend, J. Cellulose and Its Derivatives: Towards Biomedical Applications. *Cellulose* **2021**, *28* (4), 1893–1931. https://doi.org/10.1007/s10570-020-03674-w.
(12) Rahman, Md. S.; Hasan, Md. S.; Nitai, A. S.; Nam, S.; Karmakar, A. K.; Ahsan, Md. S.; Shiddiky, M. J. A.; Ahmed, M. B. Recent Developments of Carboxymethyl Cellulose. *Polymers* **2021**, *13* (8), 1345. https://doi.org/10.3390/polym13081345.
(13) Hossen, M. R.; Dadoo, N.; Holomakoff, D. G.; Co, A.; Gramlich, W. M.; Mason, M. D. Wet Stable and Mechanically Robust Cellulose Nanofibrils (CNF) Based Hydrogel. *Polymer* **2018**, *151*, 231–241. https://doi.org/10.1016/j.polymer.2018.07.016.
(14) García-Lizarribar, A.; Fernández-Garibay, X.; Velasco-Mallorquí, F.; Castaño, A. G.; Samitier, J.; Ramon-Azcon, J. Composite Biomaterials as Long-Lasting Scaffolds for 3D Bioprinting of Highly Aligned Muscle Tissue. *Macromol. Biosci.* **2018**, *18* (10), 1800167. https://doi.org/10.1002/mabi.201800167.
(15) Dutta, S.; Samanta, P.; Dhara, D. Temperature, PH and Redox Responsive Cellulose Based Hydrogels for Protein Delivery. *Int. J. Biol. Macromol.* **2016**, *87*, 92–100. https://doi.org/10.1016/j.ijbiomac.2016.02.042.
(16) Soullard, L.; Bayle, P.-A.; Lancelon-Pin, C.; Rolere, S.; Texier, I.; Jean, B.; Nonglaton, G. Optimization of the Methacrylation of Carboxymethylcellulose and Use for the Design of Hydrogels and Cryogels with Controlled Structure and Properties. *Cellulose* **2023**, *30*, 6203-6217. https://doi.org/10.1007/s10570-023-05266-w.
(17) Tomal, W.; Ortyl, J. Water-Soluble Photoinitiators in Biomedical Applications. *Polymers* **2020**, *12* (5), 1073. https://doi.org/10.3390/polym12051073.
(18) Melilli, G.; Carmagnola, I.; Tonda-Turo, C.; Pirri, F.; Ciardelli, G.; Sangermano, M.; Hakkarainen, M.; Chiappone, A. DLP 3D Printing Meets Lignocellulosic Biopolymers: Carboxymethyl Cellulose Inks for 3D Biocompatible Hydrogels. *Polymers* **2020**, *12* (8), 1655. https://doi.org/10.3390/polym12081655.
(19) Reza, A. T.; Nicoll, S. B. Characterization of Novel Photocrosslinked Carboxymethylcellulose Hydrogels for Encapsulation of Nucleus Pulposus Cells. *Acta Biomater.* **2010**, *6* (1), 179–186. https://doi.org/10.1016/j.actbio.2009.06.004.
(20) Lin, H. A.; Gupta, M. S.; Varma, D. M.; Gilchrist, M. L.; Nicoll, S. B. Lower Crosslinking Density Enhances Functional Nucleus Pulposus-like Matrix Elaboration by Human Mesenchymal Stem Cells in Carboxymethylcellulose Hydrogels: Crosslinking Density Impacts HMSC

Chondrogenesis. *J. Biomed. Mater. Res. A* **2016**, *104* (1), 165–177. https://doi.org/10.1002/jbm.a.35552.
(21) Yu, C.; Schimelman, J.; Wang, P.; Miller, K. L.; Ma, X.; You, S.; Guan, J.; Sun, B.; Zhu, W.; Chen, S. Photopolymerizable Biomaterials and Light-Based 3D Printing Strategies for Biomedical Applications. *Chem. Rev.* **2020**, *120* (19), 10695–10743. https://doi.org/10.1021/acs.chemrev.9b00810.
(22) Seo, J. W.; Kim, G. M.; Choi, Y.; Cha, J. M.; Bae, H. Improving Printability of Digital-Light-Processing 3D Bioprinting via Photoabsorber Pigment Adjustment. *Int. J. Mol. Sci.* **2022**, *23* (10), 5428. https://doi.org/10.3390/ijms23105428.
(23) Huh, J.; Moon, Y.-W.; Park, J.; Atala, A.; Yoo, J. J.; Lee, S. J. Combinations of Photoinitiator and UV Absorber for Cell-Based Digital Light Processing (DLP) Bioprinting. *Biofabrication* **2021**, *13* (3), 034103. https://doi.org/10.1088/1758-5090/abfd7a.
(24) Silva, J. da; Fracacio, R. Toxicological and Ecotoxicological Aspects of Tartrazine Yellow Food Dye: A Literature Review. *Rev. Bras. Ciênc. Ambient. Online* **2020**, *56* (1), 137–151. https://doi.org/10.5327/Z21769478746.
(25) Lin, X.; Zhao, X.; Xu, C.; Wang, L.; Xia, Y. Progress in the Mechanical Enhancement of Hydrogels: Fabrication Strategies and Underlying Mechanisms. *J. Polym. Sci.* **2022**, *60* (17), 2525–2542. https://doi.org/10.1002/pol.20220154.
(26) Chartrain, N. A.; Williams, C. B.; Whittington, A. R. A Review on Fabricating Tissue Scaffolds Using Vat Photopolymerization. *Acta Biomater.* **2018**, *74*, 90–111. https://doi.org/10.1016/j.actbio.2018.05.010.
(27) Habibi, Y.; Lucia, L. A.; Rojas, O. J. Cellulose Nanocrystals: Chemistry, Self-Assembly, and Applications. *Chem. Rev.* **2010**, *110* (6), 3479–3500. https://doi.org/10.1021/cr900339w.
(28) Moon, R. J.; Martini, A.; Nairn, J.; Simonsen, J.; Youngblood, J. Cellulose Nanomaterials Review: Structure, Properties and Nanocomposites. *Chem. Soc. Rev.* **2011**, *40* (7), 3941. https://doi.org/10.1039/c0cs00108b.
(29) Shojaeiarani, J.; Bajwa, D. S.; Chanda, S. Cellulose Nanocrystal Based Composites: A Review. *Compos. Part C Open Access* **2021**, *5*, 100164. https://doi.org/10.1016/j.jcomc.2021.100164.
(30) Favier, V.; Chanzy, H.; Cavaille, J. Y. Polymer Nanocomposites Reinforced by Cellulose Whiskers. *Macromolecules* **1995**, *28* (18), 6365–6367. https://doi.org/10.1021/ma00122a053.
(31) Dara, P. K.; Raghavankutty, M.; Deekonda, K.; Vemu, A. K.; Sivam, V.; Mathew, S.; Rangasamy, A.; Chandragiri Nagarajarao, R.; Subramanian, S. Synthesis of Biomaterial-Based Hydrogels Reinforced with Cellulose Nanocrystals for Biomedical Applications. *Int. J. Polym. Sci.* **2021**, *2021*, 1–14. https://doi.org/10.1155/2021/4865733.
(32) De France, K. J.; Hoare, T.; Cranston, E. D. Review of Hydrogels and Aerogels Containing Nanocellulose. *Chem. Mater.* **2017**, *29* (11), 4609–4631. https://doi.org/10.1021/acs.chemmater.7b00531.
(33) Cui, S.; Cui, C.; Ge, S.; Xie, W.; Yu, M.; Li, Y.; Sun, Q.; Xiong, L. The Impact of Cellulose Nanocrystals on the Rheology of Sodium Carboxymethyl Cellulose and Sodium Alginate. *J. Appl. Polym. Sci.* **2022**, *139* (38), e52919. https://doi.org/10.1002/app.52919.
(34) Oun, A. A.; Rhim, J.-W. Characterization of Carboxymethyl Cellulose-Based Nanocomposite Films Reinforced with Oxidized Nanocellulose Isolated Using Ammonium Persulfate Method. *Carbohydr. Polym.* **2017**, *174*, 484–492. https://doi.org/10.1016/j.carbpol.2017.06.121.
(35) Han, J.; Zhou, C.; Wu, Y.; Liu, F.; Wu, Q. Self-Assembling Behavior of Cellulose Nanoparticles during Freeze-Drying: Effect of Suspension Concentration, Particle Size, Crystal Structure, and Surface Charge. *Biomacromolecules* **2013**, *14* (5), 1529–1540. https://doi.org/10.1021/bm4001734.
(36) Cafiso, D.; Septevani, A. A.; Noè, C.; Schiller, T.; Pirri, C. F.; Roppolo, I.; Chiappone, A. 3D Printing of Fully Cellulose-Based Hydrogels by Digital Light Processing. *Sustain. Mater. Technol.* **2022**, *32*, e00444. https://doi.org/10.1016/j.susmat.2022.e00444.
(37) Brinatti, C.; Akhlaghi, S. P.; Pires-Oliveira, R.; Bernardinelli, O. D.; Berry, R. M.; Tam, K. C.; Loh, W. Controlled Coagulation and Redispersion of Thermoresponsive Poly Di(Ethylene Oxide)

Methyl Ether Methacrylate Grafted Cellulose Nanocrystals. *J. Colloid Interface Sci.* **2019**, *538*, 51–61. https://doi.org/10.1016/j.jcis.2018.11.071.

(38) Qu, Z.; Schueneman, G. T.; Shofner, M. L.; Meredith, J. C. Acrylic Functionalization of Cellulose Nanocrystals with 2-Isocyanatoethyl Methacrylate and Formation of Composites with Poly(Methyl Methacrylate). *ACS Omega* **2020**, *5* (48), 31092–31099. https://doi.org/10.1021/acsomega.0c04246.

(39) Wang, B.; Liu, J.; Chen, K.; Wang, Y.; Shao, Z. Three-Dimensional Printing of Methacrylic Grafted Cellulose Nanocrystal-Reinforced Nanocomposites With Improved Properties. *Polym. Eng. Sci.* **2020**, *60* (4), 782–792. https://doi.org/10.1002/pen.25336.

(40) Wang, J.; Siqueira, G.; Müller, G.; Rentsch, D.; Huch, A.; Tingaut, P.; Levalois-Grützmacher, J.; Grützmacher, H. Synthesis of New Bis(Acyl)Phosphane Oxide Photoinitiators for the Surface Functionalization of Cellulose Nanocrystals. *Chem. Commun.* **2016**, *52* (13), 2823–2826. https://doi.org/10.1039/C5CC09760F.

(41) Bai, H.; Li, Y.; Zhang, S.; Ma, P.; Dong, W. Photo-crosslinkable Poly (Vinyl Alcohol)/Nanocrystalline Cellulose Composites with Controllable Performance and Exceptional Water Vapor Barrier Property for Packaging Application. *Cellulose* **2022**, *29*, 7721–7734. https://doi.org/t https://doi. org/10.1007/s10570-022-04760-x.

(42) Siqueira, G.; Kokkinis, D.; Libanori, R.; Hausmann, M. K.; Gladman, A. S.; Neels, A.; Tingaut, P.; Zimmermann, T.; Lewis, J. A.; Studart, A. R. Cellulose Nanocrystal Inks for 3D Printing of Textured Cellular Architectures. *Adv. Funct. Mater.* **2017**, *27* (12), 1604619. https://doi.org/10.1002/adfm.201604619.

(43) Müller, L. A. E.; Demongeot, A.; Vaucher, J.; Leterrier, Y.; Avaro, J.; Liebi, M.; Neels, A.; Burgert, I.; Zimmermann, T.; Nyström, G.; Siqueira, G. Photoresponsive Movement in 3D Printed Cellulose Nanocomposites. *ACS Appl. Mater. Interfaces* **2022**, *14* (14), 16703–16717. https://doi.org/10.1021/acsami.2c02154.

(44) Kelly, P. V.; Cheng, P.; Gardner, D. J.; Gramlich, W. M. Aqueous Polymer Modification of Cellulose Nanofibrils by Grafting-Through a Reactive Methacrylate Group. *Macromol. Rapid Commun.* **2021**, *42* (3), 2000531. https://doi.org/10.1002/marc.202000531.

(45) Ma, Q.; Mohawk, D.; Jahani, B.; Wang, X.; Chen, Y.; Mahoney, A.; Zhu, J. Y.; Jiang, L. UV-Curable Cellulose Nanofiber-Reinforced Soy Protein Resins for 3D Printing and Conventional Molding. *ACS Appl. Polym. Mater.* **2020**, *2* (11), 4666–4676. https://doi.org/10.1021/acsapm.0c00717.

(46) Revol, J.-F.; Bradford, H.; Giasson, J.; Marchessault, R. H.; Gray, D. G. Helicoidal Self-Ordering of Cellulose Microfibrils in Aqueous Suspension. *Int. J. Biol. Macromol.* **1992**, *14* (3), 170–172. https://doi.org/10.1016/S0141-8130(05)80008-X.

(47) Eyley, S.; Thielemans, W. Surface Modification of Cellulose Nanocrystals. *Nanoscale* **2014**, *6*(14), 7764-7779. https://doi-org/10.1039/C4NR01756K

(48) Azzam, F.; Frka-Petesic, B.; Semeraro, E. F.; Cousin, F.; Jean, B. Small-Angle Neutron Scattering Reveals the Structural Details of Thermosensitive Polymer-Grafted Cellulose Nanocrystal Suspensions. *Langmuir* **2020**, *36* (29), 8511–8519. https://doi.org/10.1021/acs.langmuir.0c01103.

(49) Nishiyama, Y.; Langan, P.; Chanzy, H. Crystal Structure and Hydrogen-Bonding System in Cellulose Iβ from Synchrotron X-Ray and Neutron Fiber Diffraction. *J. Am. Chem. Soc.* **2002**, *124* (31), 9074–9082. https://doi.org/10.1021/ja0257319.

(50) Darpentigny, C.; Molina-Boisseau, S.; Nonglaton, G.; Bras, J.; Jean, B. Ice-Templated Freeze-Dried Cryogels from Tunicate Cellulose Nanocrystals with High Specific Surface Area and Anisotropic Morphological and Mechanical Properties. *Cellulose* **2020**, *27* (1), 233–247. https://doi.org/10.1007/s10570-019-02772-8.

(51) Niskanen, I.; Suopajärvi, T.; Liimatainen, H.; Fabritius, T.; Heikkilä, R.; Thungström, G. Determining the Complex Refractive Index of Cellulose Nanocrystals by Combination of Beer-Lambert and Immersion Matching Methods. *J. Quant. Spectrosc. Radiat. Transf.* **2019**, *235*, 1–6. https://doi.org/10.1016/j.jqsrt.2019.06.023.

(52) I.S. EN ISO 10993-5: Biological Evaluation of Medical Devices - Part 5: Tests for in Vitro Cytotoxicity.

(53) Atalla, R. H.; VanderHart, D. L. The Role of Solid State 13C NMR Spectroscopy in Studies of the Nature of Native Celluloses. *Solid State Nuclear Magnetic Resonance*, **1999**, *15*, 1-19.

(54) Gårdebjer, S.; Bergstrand, A.; Idström, A.; Börstell, C.; Naana, S.; Nordstierna, L.; Larsson, A. Solid-State NMR to Quantify Surface Coverage and Chain Length of Lactic Acid Modified Cellulose Nanocrystals, Used as Fillers in Biodegradable Composites. *Compos. Sci. Technol.* **2015**, *107*, 1–9. https://doi.org/10.1016/j.compscitech.2014.11.014.

(55) Isogai, A.; Usuda, M.; Kato, T.; Uryu, T.; Atalla, R. H. Solid-State CP/MAS Carbon-13 NMR Study of Cellulose Polymorphs. *Macromolecules* **1989**, *22* (7), 3168–3172. https://doi.org/10.1021/ma00197a045.

(56) Haouache, S.; Jimenez-Saelices, C.; Cousin, F.; Falourd, X.; Pontoire, B.; Cahier, K.; Jérome, F.; Capron, I. Cellulose Nanocrystals from Native and Mercerized Cotton. *Cellulose* **2022**, *29* (3), 1567–1581. https://doi.org/10.1007/s10570-021-04313-8.

(57) Park, S.; Baker, J. O.; Himmel, M. E.; Parilla, P. A.; Johnson, D. K. Cellulose Crystallinity Index: Measurement Techniques and Their Impact on Interpreting Cellulase Performance. *Biotechnology for biofuels* **2010**, *3*, 1-10. https://doi-org/10.1186/1754-6834-3-10

(58) Pandi, Narsimha.; Sonawane, S. H.; Anand Kishore, K. Synthesis of Cellulose Nanocrystals (CNCs) from Cotton Using Ultrasound-Assisted Acid Hydrolysis. *Ultrason. Sonochem.* **2021**, *70*, 105353. https://doi.org/10.1016/j.ultsonch.2020.105353.

(59) Johnson, R. L.; Schmidt-Rohr, K. Quantitative Solid-State 13C NMR with Signal Enhancement by Multiple Cross Polarization. *J. Magn. Reson.* **2014**, *239*, 44–49. https://doi.org/10.1016/j.jmr.2013.11.009.

(60) Jordan, J. H.; Easson, M. W.; Condon, B. D. Alkali Hydrolysis of Sulfated Cellulose Nanocrystals: Optimization of Reaction Conditions and Tailored Surface Charge. *Nanomaterials* **2019**, *9* (9), 1232. https://doi.org/10.3390/nano9091232.

(61) Pandey, A.; Derakhshandeh, M.; Kedzior, S. A.; Pilapil, B.; Shomrat, N.; Segal-Peretz, T.; Bryant, S. L.; Trifkovic, M. Role of Interparticle Interactions on Microstructural and Rheological Properties of Cellulose Nanocrystal Stabilized Emulsions. *J. Colloid Interface Sci.* **2018**, *532*, 808–818. https://doi.org/10.1016/j.jcis.2018.08.044.

(62) Kloser, E.; Gray, D. G. Surface Grafting of Cellulose Nanocrystals with Poly(Ethylene Oxide) in Aqueous Media. *Langmuir* **2010**, *26* (16), 13450–13456. https://doi.org/10.1021/la101795s.

(63) Lam, E.; Hemraz, U. D. Preparation and Surface Functionalization of Carboxylated Cellulose Nanocrystals. *Nanomaterials* **2021**, *11* (7), 1641. https://doi.org/10.3390/nano11071641.

(64) Zandrini, T.; Liaros, N.; Jiang, L. J.; Lu, Y. F.; Fourkas, J. T.; Osellame, R.; Baldacchini, T. Effect of the Resin Viscosity on the Writing Properties of Two-Photon Polymerization. *Opt. Mater. Express* **2019**, *9* (6), 2601. https://doi.org/10.1364/OME.9.002601.

(65) Hassan, M. L.; Zeid, R. E. A.; Fadel, S. M.; Sakhawy, M. E.; Khiari, R. Cellulose Nanocrystals and Carboxymethyl Cellulose from Olive Stones and Their Use to Improve Paper Sheets Properties. *Int. J. Nanoparticles* **2014**, *7* (3/4), 261. https://doi.org/10.1504/IJNP.2014.067613.

(66) da Fonsêca, J. H. L.; d'Ávila, M. A. Rheological Behavior of Carboxymethylcellulose and Cellulose Nanocrystal Aqueous Dispersions. *Rheol. Acta* **2021**, *60* (9), 497–509. https://doi.org/10.1007/s00397-021-01292-2.

(67) Azrak, S. M. E. A.; Gohl, J. A.; Moon, R. J.; Schueneman, G. T.; Davis, C. S.; Youngblood, J. P. Controlled Dispersion and Setting of Cellulose Nanofibril - Carboxymethyl Cellulose Pastes. *Cellulose* **2021**, *28* (14), 9149–9168. https://doi.org/10.1007/s10570-021-04081-5.

(68) Butchosa, N.; Zhou, Q. Water Redispersible Cellulose Nanofibrils Adsorbed with Carboxymethyl Cellulose. *Cellulose* **2014**, *21* (6), 4349–4358. https://doi.org/10.1007/s10570-014-0452-7.

(69) Bhattacharjee, N.; Parra-Cabrera, C.; Kim, Y. T.; Kuo, A. P.; Folch, A. Desktop-Stereolithography 3D-Printing of a Poly(Dimethylsiloxane)-Based Material with Sylgard-184 Properties. *Adv. Mater.* **2018**, *30* (22), 1800001. https://doi.org/10.1002/adma.201800001.
(70) Kowalonek, J.; Kaczmarek, H.; Kurzawa, M. Effect of UV-Irradiation on Fluorescence of Poly(Methyl Methacrylate) Films with Photosensitive Organic Compounds. *J. Photochem. Photobiol. Chem.* **2016**, *319–320*, 18–24. https://doi.org/10.1016/j.jphotochem.2015.12.017.
(71) Miedzińska, D.; Gieleta, R.; Popławski, A. Experimental Study on Influence of Curing Time on Strength Behavior of SLA-Printed Samples Loaded with Different Strain Rates. *Materials* **2020**, *13* (24), 5825. https://doi.org/10.3390/ma13245825.
(72) Yoshii, E. Cytotoxic Effects of Acrylates and Methacrylates: Relationships of Monomer Structures and Cytotoxicity. *J. Biomed. Mater. Res.* **1997**, *37* (4), 517–524. https://doi.org/10.1002/(SICI)1097-4636(19971215)37:4<517::AID-JBM10>3.0.CO;2-5.
(73) Yang, J.; Han, C.-R.; Duan, J.-F.; Xu, F.; Sun, R.-C. Mechanical and Viscoelastic Properties of Cellulose Nanocrystals Reinforced Poly(Ethylene Glycol) Nanocomposite Hydrogels. *ACS Appl. Mater. Interfaces* **2013**, *5* (8), 3199–3207. https://doi.org/10.1021/am4001997.
(74) Mantha, S.; Pillai, S.; Khayambashi, P.; Upadhyay, A.; Zhang, Y.; Tao, O.; Pham, H. M.; Tran, S. D. Smart Hydrogels in Tissue Engineering and Regenerative Medicine. *Materials* **2019**, *12* (20), 3323. https://doi.org/10.3390/ma12203323.
(75) Abbasi, N.; Hamlet, S.; Love, R. M.; Nguyen, N.-T. Porous Scaffolds for Bone Regeneration. *J. Sci. Adv. Mater. Devices* **2020**, *5* (1), 1–9. https://doi.org/10.1016/j.jsamd.2020.01.007.
(76) Sindhu, K. A.; Prasanth, R.; Thakur, V. K. Medical Applications of Cellulose and Its Derivatives: Present and Future. In *Nanocellulose Polymer Nanocomposites*; Thakur, V. K., Ed.; John Wiley & Sons, Inc.: Hoboken, NJ, USA, 2014; pp 437–477. https://doi.org/10.1002/9781118872246.ch16.
(77) Tyshkunova, I. V.; Poshina, D. N.; Skorik, Y. A. Cellulose Cryogels as Promising Materials for Biomedical Applications. *Int. J. Mol. Sci.* **2022**, *23* (4), 2037. https://doi.org/10.3390/ijms23042037.
(78) Hoare, T. R.; Kohane, D. S. Hydrogels in Drug Delivery: Progress and Challenges. *Polymer* **2008**, *49* (8), 1993–2007. https://doi.org/10.1016/j.polymer.2008.01.027.

- For Table of Contents Only